

ARTICLE

Open Access

Mithramycin selectively attenuates DNA-damage-induced neuronal cell death

Oleg Makarevich¹, Boris Sabirzhanov¹, Taryn G. Aubrecht¹, Ethan P. Glaser¹, Brian M. Polster¹, Rebecca J. Henry¹, Alan I. Faden¹ and Bogdan A. Stoica¹

Abstract

DNA damage triggers cell death mechanisms contributing to neuronal loss and cognitive decline in neurological disorders, including traumatic brain injury (TBI), and as a side effect of chemotherapy. Mithramycin, which competitively targets chromatin-binding sites of specificity protein 1 (Sp1), was used to examine previously unexplored neuronal cell death regulatory mechanisms via rat primary neurons *in vitro* and after TBI in mice (males). In primary neurons exposed to DNA-damage-inducing chemotherapy drugs *in vitro* we showed that DNA breaks sequentially initiate DNA-damage responses, including phosphorylation of ATM, H₂AX and tumor protein 53 (p53), transcriptional activation of pro-apoptotic BH3-only proteins, and mitochondrial outer membrane permeabilization (MOMP), activating caspase-dependent and caspase-independent intrinsic apoptosis. Mithramycin was highly neuroprotective in DNA-damage-dependent neuronal cell death, inhibiting chemotherapeutic-induced cell death cascades downstream of ATM and p53 phosphorylation/activation but upstream of p53-induced expression of pro-apoptotic molecules. Mithramycin reduced neuronal upregulation of BH3-only proteins and mitochondrial dysfunction, attenuated caspase-3/7 activation and caspase substrates' cleavage, and limited c-Jun activation. Chromatin immunoprecipitation indicated that mithramycin attenuates Sp1 binding to pro-apoptotic gene promoters without altering p53 binding suggesting it acts by removing cofactors required for p53 transactivation. In contrast, the DNA-damage-independent neuronal death models displayed caspase initiation in the absence of p53/BH3 activation and were not protected even when mithramycin reduced caspase activation. Interestingly, experimental TBI triggers a multiplicity of neuronal death mechanisms. Although markers of DNA-damage/p53-dependent intrinsic apoptosis are detected acutely in the injured cortex and are attenuated by mithramycin, these processes may play a reduced role in early neuronal death after TBI, as caspase-dependent mechanisms are repressed in mature neurons while other, mithramycin-resistant mechanisms are active. Our data suggest that Sp1 is required for p53-mediated transactivation of neuronal pro-apoptotic molecules and that mithramycin may attenuate neuronal cell death in conditions predominantly involving DNA-damage-induced p53-dependent intrinsic apoptosis.

Introduction

Annually, over 4 million people in the US are impacted by traumatic brain injury (TBI)¹ and almost 40% of patients demonstrate persistent functional decline². TBI triggers multiple secondary injury processes leading to

progressive neurodegeneration and related neurological deficits^{3–5}. Increased production and accumulation of reactive oxygen species after TBI is a key secondary injury mechanism and can result in significant DNA damage and subsequent apoptosis⁶. Neurological dysfunctions are also a common side effect of cancer therapy with a substantial subset of patients suffering from chemotherapy-related cognitive impairment or “chemobrain”⁷. Drug-induced DNA damage and secondary central neurotoxicity may

Correspondence: Bogdan A. Stoica (bstoica@som.umaryland.edu)

¹Department of Anesthesiology and Shock, Trauma and Anesthesiology Research (STAR) Center, University of Maryland School of Medicine, Baltimore, MD 21201, USA

Edited by M. Agostini

© The Author(s) 2020



Open Access This article is licensed under a Creative Commons Attribution 4.0 International License, which permits use, sharing, adaptation, distribution and reproduction in any medium or format, as long as you give appropriate credit to the original author(s) and the source, provide a link to the Creative Commons license, and indicate if changes were made. The images or other third party material in this article are included in the article's Creative Commons license, unless indicated otherwise in a credit line to the material. If material is not included in the article's Creative Commons license and your intended use is not permitted by statutory regulation or exceeds the permitted use, you will need to obtain permission directly from the copyright holder. To view a copy of this license, visit <http://creativecommons.org/licenses/by/4.0/>.

play a key role in cognitive impairments after chemotherapy⁸.

The intrinsic apoptosis pathway initiated by DNA damage⁹ involves p53 phosphorylation at serine 15^{10,11}, followed by p53-dependent transcriptional activation of pro-apoptotic Bcl-2 family members^{12,13}. These changes cause mitochondrial release^{14,15} of pro-apoptotic molecules such as cytochrome c (CytC) and apoptosis-inducing factor (AIF), leading to caspase-dependent and caspase-independent intrinsic apoptosis, respectively^{10,15–17}. Experimental TBI models have also been associated with the production of single- and double-strand breaks in DNA and the resulting p53 activation contributes to neuronal loss and associated neurological deficits^{18,19}. Accordingly, various studies have shown that p53 inhibition is neuroprotective^{10,16,20–22}. However, p53 has also been shown to induce the expression of molecules required for neurite outgrowth and axonal regeneration and may promote regenerative responses following central nervous system injuries²³. Thus, it is essential to separate maladaptive responses contributing to the neuropathology from adaptive responses enabling neuronal survival²⁴. Total inhibition of p53 activities may be deleterious²⁵, and an effective long-term strategy requires a more selective modulation of p53's transcriptional effects.

Specificity protein 1 (Sp1) may regulate p53's transcriptional profile and ability to promote apoptosis after DNA damage^{26,27}. Furthermore, Sp1 can synergistically transactivate p53-binding promoters and may be necessary for p53-induced promoter transactivation²⁸.

To examine the role of Sp1 in DNA-damage-induced neuronal apoptosis, a p53-transcription-dependent pathway, we utilized mithramycin, a drug that binds G–C-rich DNA to compete with Sp1 chromatin binding²⁹ and has neuroprotective effects in several models involving p53 activation, including ischemic injury²⁹, Huntington's disease³⁰, and spinal cord injury³¹. Pivotal studies by Ratan et al. showed that mithramycin inhibits apoptosis in models of DNA damage and oxidative stress *in vitro*^{32,33}. However, no previous studies have comprehensively probed mithramycin's mechanisms of action and examined its effects in DNA-damage-dependent and -independent neuronal intrinsic apoptosis models *in vitro* as well as after experimental TBI *in vivo*. We investigated mithramycin's ability to attenuate specific cell death mechanisms activated in various models of neuronal death and to promote neuronal survival.

Materials and methods

Neuronal cell death and cell viability assays

Cell death was measured via LDH release (cytosolic LDH is released from dying cells due to membrane permeabilization) using the LDH-GloTM Cytotoxicity Assay (Cat. #J2380 Promega, Madison, WI) by combining 10 μ L

of media from a 96-well plate well with 10 μ L of detection enzyme and reductase substrate, premixed just before assaying in the proportion recommended in the protocol and then diluted 1:10 in LDH Storage Buffer (also prepared as recommended in the protocol)³⁴. Luminescence was measured after 1-h incubation in the dark in a BioTek Synergy HT Plate Reader using Gen5TM software.

Calcein AM assay (Cat. #ALX-610-026, Enzo Life Sciences, Farmingdale, NY) was used to measure cell viability (calcein AM is retained in the cytosol of viable cells due to membrane integrity). Briefly, 1 mM stock of reagent in DMSO was added to pre-warmed Locke's buffer (154 mM NaCl, 5.6 mM KCl, 3.6 mM NaHCO₃, 5.6 mM glucose, 2.3 mM CaCl₂, 5 mM HEPES, 1.2 mM MgCl₂, pH 7.3) to a final concentration of 5 μ M. Media was aspirated from 96-well plates and 100 μ L of 5 μ M calcein AM in Locke's buffer was added to each well. Plates were incubated at 37 °C for 30 min after which fluorescent signal (excitation: 485 nm, emission: 528 nm) was read in a BioTek Synergy HT Plate Reader using Gen5TM software.

Primary cortical neuronal cultures

Embryonal rat cortical neurons (RCN) were derived as previously described from rat E15-16 cortices³⁵. For each experiment, cortices were obtained from all embryos (mixed, unknown sex) of a single pregnant Sprague-Dawley® dam (Envigo). After dissociation, cells were seeded onto 96-well, 12-well, 60 mm, 100 mm cell culture plates (Corning, Corning, NY) or XF24 cell culture microplates (Agilent, Santa Clara, CA) and maintained in serum-free conditions using the B27 supplement (ThermoFisher, Waltham, MA) as described previously³⁵. We previously showed these cultures are >90% neuronal³⁶.

Etoposide (Cat. #BML-GR307, Enzo Life Sciences, Farmingdale, NY), staurosporine (Cat. #ALX-380-014, Enzo Life Sciences, Farmingdale, NY), camptothecin (Cat. #ALX-350-015, Enzo Life Sciences, Farmingdale, NY), C₂-ceramide (Cat. #BML-SL100, Enzo Life Sciences, Farmingdale, NY), doxorubicin (Cat. #CST-5927, Cell Signaling Technologies, Danvers, MA), and mithramycin (Cat. #11434, Cayman Chemical Company, Ann Arbor, MI) were used to treat 7 days *in vitro* (DIV) cells at concentrations and for times indicated elsewhere.

Mitochondrial respiration measurement

After 6 h treatment in a XF24 cell culture microplate (Agilent, Santa Clara, CA), mitochondrial oxygen consumption rate (OCR) was measured by utilizing an Agilent Seahorse XF Analyzer as previously described^{37,38}. Briefly, after 6 h treatment of RCN with etoposide +/- mithramycin, 0.5 μ g/ml oligomycin, 200 μ M dinitrophenol, 10 mM pyruvate, and 1 μ M antimycin A were sequentially added to identify maximum and spare respiratory capacities. Pyruvate was added to ensure that

endogenous substrate was not the limiting factor in maximal respiration measurements. Treatment length was chosen because time course analysis of LDH release (data not shown) indicated little to no cell death occurring 6 h after etoposide treatment.

RNA isolation and quantitative qPCR

Total RNA was isolated using either the miRNeasy kit (QIAGEN, Hilden, Germany) or the Zymo Research Direct-zol RNA kits (Zymo Research, Irvine, CA) according to the manufacturers' protocols. Either the Verso cDNA Synthesis kit (Cat. #AB1453B, ThermoFisher, Waltham, MA) or the High-Capacity cDNA Reverse Transcription kit (Cat. #4368813, ThermoFisher, Waltham, MA) was used to synthesize cDNA from purified RNA based on the manufacturer's protocol. Quantitative real-time PCR was performed using TaqMan Universal Master Mix II (Applied Biosystems, Foster City, CA) with 50 ng cDNA per sample, in duplicate, using the following TaqManTM primers: Bbc3/PUMA: Rn00597992_m1; Pmaip1/Noxa: Rn01494552_m1; Cdkn1a/p21: Rn01427989_s1; Akt1: Rn00583646_m1; Ang-1: Rn01504818_m1.

Reactions were amplified and quantified via an Applied Biosystems QuantStudio 5 and its corresponding software (Applied Biosystems, Foster City, CA). The PCR profile consisted of one cycle of 50 °C for 2 min and 95 °C for 10 min, followed by 40 cycles of 95 °C for 15 s and 60 °C for 1 min. Gene expression was normalized to GAPDH and the relative quantities of mRNA calculated using the 2^{-ddCt} method as described previously³⁹.

MicroRNA reverse transcription and qPCR

100 ng/sample of total RNA was isolated as described above and reverse transcribed using TaqManTM MicroRNA Reverse Transcription Kit (Cat #4366596, ThermoFisher, Waltham, MA) and TaqManTM primers. Equal volumes of each sample were loaded in duplicate for qPCR using TaqManTM Advanced miRNA assays and the following primers: miR-711: Cat. #241136_mat; miR-23a: Cat. #000319.

Reactions were amplified and quantified via an Applied Biosystems QuantStudio 5 and its corresponding software (Applied Biosystems, Foster City, CA). The PCR profile consisted of one cycle of 50 °C for 2 min and 95 °C for 10 min, followed by 40 cycles of 95 °C for 15 s and 60 °C for 1 min. Gene expression was normalized to U6 small nucleolar RNA and the relative quantities of miRNA calculated using the 2^{-ddCt} method as described previously³⁹.

Cell lysate preparation and western blot

After 24 h (or less) treatment of RCN with cell death inducer +/- mithramycin, cells were quickly scraped from the dish and added to cold 1X PBS. The mixture was

centrifuged at 1000 × g to pellet cells and supernatant was removed. RIPA buffer (Cat #R3792, Teknova, Hollister, CA) with Protease Inhibitor and Phosphatase Inhibitor (2,3) cocktails (Sigma-Aldrich, St. Louis, MO) was added to the pellet and complete lysis was ensured by incubating the lysate at 4 °C with rocking for 30 min and vortexing thoroughly every 10 min during the incubation. To ensure appropriate comparisons between samples, we took the two-pronged approach of both loading equal amounts of protein and normalizing to an appropriate housekeeping protein. Protein concentration was measured using PierceTM BCA Protein Assay Kit (ThermoFisher, Waltham, MA) according to the manufacturer's instructions. Equal amounts of protein were loaded onto 4–20% CriterionTM TGXTM Precast Midi Protein Gels (Bio-Rad, Hercules, CA) and electrophoresis was performed. Proteins were transferred to 0.2 μm nitrocellulose membranes using the Trans-Blot® TurboTM (Bio-Rad, Hercules, CA). Membranes were washed, incubated with primary and secondary antibodies (see antibody list), and complexes were visualized using SuperSignalTM West Dura Extended Duration Substrate (ThermoFisher, Waltham, MA). To assess proteins with sufficiently separate molecular weights, membranes were cut into sections and probed separately using supplier-validated antibodies.

Chemiluminescence was captured on a ChemiDocTM Touch Imaging System (Bio-Rad, Hercules, CA) and protein bands were quantified by densitometric analysis using ImageLab software (Bio-Rad, Hercules, CA). Images were acquired under non-saturating conditions and were normalized to an endogenous control for each sample (arbitrary units). When membranes were sectioned for separate analysis, each section was normalized to the endogenous control from the same membrane. All quantifications are presented after normalization.

Subcellular fractionation

Subcellular fractionation was performed as described previously³⁶. Briefly, RCN were harvested and washed in ice-cold phosphate-buffered saline. The cell suspension was centrifuged at 500 × g for 15 min at 4 °C. The cell pellet was resuspended for 10 min on ice in digitonin lysis buffer (20 mM HEPES, pH 7.4, 80 mM KCl, 1 mM EDTA, 1 mM EGTA, 1 mM DTT, 250 mM sucrose, 200 μg/mL digitonin, and protease inhibitor and phosphatase inhibitor (2,3) cocktails (Sigma-Aldrich, St. Louis, MO)). Cells were passaged 20 times through a 22G needle. The lysate was centrifuged at 1000 × g for 5 min at 4 °C to pellet the nuclei. The supernatant was transferred to a new tube and centrifuged again at 12,000 × g for 10 min at 4 °C to pellet the mitochondria. The resulting supernatant, representing the cytosolic fraction, was recovered. Nuclear and mitochondrial lysates were prepared in RIPA buffer

(Cat #R3792, Teknova, Hollister, CA) with protease inhibitor and phosphatase inhibitor (2,3) cocktails (Sigma-Aldrich). All steps were performed on ice. Pooled nuclear, cytosolic and total lysates were probed via electrophoresis and western blot for COX IV to identify mitochondrial content and Lamin to identify nuclear content to verify fractionation procedure.

Chromatin immunoprecipitation (ChIP)

ChIP assay was performed as previously described³⁷ using a kit from Epigentek (Farmlandale, NY), with 2 µg of antibodies to p53 or 4 µg of antibodies to Sp1 per sample. Briefly, after cross-linking using 1% formaldehyde in PBS, cells were lysed and chromatin sheared to generate fragments from 200 to 600 bp using a Bioruptor sonicator (Diagenode). After this, immunoprecipitation was performed. The following binding sites were analyzed using the following primer sequences (all nt locations from Rnor_6.0 chromosome 18). Primers were ordered from Integrated DNA Technologies (Coralville, Iowa).

Primers:

5'-CTTCCCTCCCACCTTCGTTT-3'

(62,174,414 –62,174,434 nt)

5'-GCCGGCTCTCGGGTTTTAT-3'

(62,174,653–62,174,872 nt)

p53 site: 5'-CGGCTTGCCCCGGCAAGTTG-3' (62,174,513–62,174,533 nt)

Sp1 site: 5'-TTCGAAGGGGCGGGG-3' (62,174,589–62,174,604 nt).

Rat negative control primer set 1 (Active Motif) was also used to amplify a fragment of a gene desert on rat chromosome 3 as a negative control. Normal rabbit IgG (#3900 Cell Signaling Technologies, Danvers, MA) and anti-RNA polymerase II antibody (Epigentek, Farmingdale, NY) were used as negative and positive controls to validate the primer set used on both IPs. The difference between the negative control IP and the average sample IP was 21.8-fold, while the difference between the positive control IP and the average sample IP was 3.33-fold. A dilution series was utilized to calculate the reaction efficiency, and it was found to be 77.1% for our primer pair. Relative expression was calculated using the Pfaffl method⁴⁰.

Immunocytochemistry

For the phospho-c-Jun (S73) time course, RCN were treated with etoposide +/- mithramycin on DIV 7 in 24-well plates with coverslips. After 6, 12, or 24 h, cells were fixed for 10 min in 4% paraformaldehyde/PBS and co-stained with a 1:200 dilution of Cell Signaling's phospho-c-Jun (S73) and a 1:400 dilution of Millipore's Milli-MarkTM Pan-Neuronal Marker in 10% goat serum (Gemini Bio-Products, West Sacramento, CA) overnight. Wells were incubated the next day with goat-derived

secondary antibody (Life Technologies, Fisher Scientific, Hampton, NH), followed by 4',6-diamidino-2-phenylindole (DAPI, Sigma-Aldrich, St. Louis, MO) (0.5 µg/mL in saline). Imaging was performed via a Leica SP5 II confocal microscope using a ×20 dry objective and ×63 oil-immersion objective. Settings were optimized to maximize signal intensity in controls without oversaturating signal in higher-intensity samples (etoposide-treated). Analysis was done using an ImageJ macro as described previously³⁷ to generate an unbinned cumulative frequency distribution plotting intensity of phospho-c-Jun (S73) signal per cell.

For the phospho-p53 (S15) assessment at 6 h, RCN were treated with etoposide +/- mithramycin or Mithramycin alone on DIV 7 in 24-well plates with coverslips. After 6 h, cells were fixed and stained with Abcam's phospho-p53 (S15) antibody. Imaging was performed via a Nikon Ti-E fluorescent microscope using a ×63 oil-immersion objective. Analysis was performed using Nikon's NIS-Elements software to generate an unbinned cumulative frequency distribution plotting intensity of phospho-p53 (S15) signal per cell.

To compare cell death inducers, RCN were treated with doxorubicin, etoposide, C₂-ceramide, staurosporine +/- mithramycin on DIV 7 in 24-well plates with coverslips. After 6 h, cells were fixed and co-stained as described above with a 1:200 dilution of Cell Signaling's cleaved PARP (94885), cleaved Casp3 (9664) or phospho-c-Jun (S73) antibodies and Millipore's Milli-MarkTM antibody. Imaging was performed via a Nikon Ti-E fluorescent microscope using a ×63 oil-immersion objective. Analysis was performed via Nikon's NIS-Elements software to generate an unbinned cumulative frequency distribution plotting intensity of phospho-c-Jun (S73) signal per cell. It was also used for identifying total cleaved PARP or cleaved Casp3 signal per field (normalized to the number of nuclei per field) for quantification of cleaved PARP and cleaved Casp3.

Antibodies

Various antibodies from different vendors were used in this study.

Cell Signaling (Danvers, MA): PARP (9542); cleaved PARP [Asp214, 89 kDa fragment] (9545/94885); cleaved Casp3 [Asp175, 17 kDa fragment] (9661/9664); cleaved Casp7 [20 kDa fragment] (9492); phospho-H₂AX (S139) (9718); phospho-p53 (S15) (12571); total p53 for ChIP (32532); PUMA (14570); AIF (4642); cytochrome c oxygenase IV (COX IV) (4884); Lamin A/C (4777); phospho-c-Jun (S63) (2361); phospho-c-Jun (S73) (3270); total c-Jun (9165); total c-Fos (2250). Millipore (Ontario, Canada): phospho-ATM(S1981) (05-740); Sp1 for ChIP (07-645); p21—mouse samples (188224); Milli-MarkTM Pan-Neuronal Marker (MAB2300). BD Biosciences (San

Jose, CA): p21—rat samples (556430). Sigma-Aldrich (St. Louis, MO): β -actin: A1978. Santa Cruz (Dallas, TX): cytochrome c (sc-13560). Enzo (Farmingdale, NY): α -Fodrin or α II-spectrin (a subunit of Fodrin, also known as “brain spectrin”)⁴¹: BML-FG6090. Abcam (Cambridge, MA): phospho-p53 (ab1431).

Mice

Eight-week-old (20–25 g) male C57BL/6 mice were obtained from JAX (Jackson Laboratories, Bar Harbor, ME) for the in vivo experiments. Mice were maintained in a 12-h light/dark cycle with ad libitum access to food and water. All activities were in accordance with protocols approved by the University of Maryland School of Animal Care and Use Committee and complied with the Guide for the Care and Use of Laboratory Animals published by NIH (DHEW publication NIH 85-23-2985).

Controlled cortical impact

We utilized a custom-designed CCI injury device^{37,42,43} consisting of a microprocessor-controlled pneumatic impactor with a 3.5 mm diameter tip. Mice were anesthetized with isoflurane (3–3.5% induction, 1.5% maintenance) in a 70% NO₂, 30% O₂ gas mixture administered via nose mask. Animals were monitored during procedures to assess depth of anesthesia via respiration rate and pedal withdrawal reflexes. The surgical site was clipped, then the head mounted in a stereotaxic frame and the injury site cleaned with betadine (Professional Disposables, Orangebury, NY) and ethanol scrubs (Fisher Scientific, Hampton, NH). Mice received puralube vet ointment eye lubrication (Dechra Veterinary Products, Overland Park, KS). A 10-mm midline incision was made over the skull, the skin and fascia were reflected, and a 5 mm craniotomy was made on the central aspect of the left parietal bone^{37,44}. The impactor tip of the injury device was extended to its full stroke distance (44 mm) and positioned to the surface of the exposed dura, then reset to impact the cortical surface. Moderate injury was performed using impactor velocity of 6 m/s and deformation depth of 2 mm, as previously described⁴⁵. The incision was then closed via 6 mm nylon surgical sutures (Unify® Premium+, AD Surgical, Sunnyvale, CA) and anesthesia was terminated. Mice were randomly assigned to CCI or sham groups. Sham mice underwent only anesthesia and incision (with no craniotomy).

Drug administration

Following injury, mice received an intracerebroventricular (icv) injection of 0.3 mM mithramycin in artificial CSF (#59-7316, Harvard Apparatus, Holliston, MA) or equal volume of vehicle (artificial CSF + DMSO). Solutions were prepared on the day of surgery. The injection was performed immediately after injury via 30-gauge

needle attached to Hamilton syringe (Hamilton, Reno, NV) into the left ventricle (anterior posterior (AP): –0.5, medial lateral (ML): –1.0, dorsal ventral (DV): –2.0 from bregma) at a rate of 0.5 μ L/min with a final volume of 5 μ L (1.5 nmoles) infused over 10 min. This dose was based on prior work utilizing CR8³⁷, and comparisons of the two compounds' neuroprotective effects in vitro. CCI mice were randomly assigned to an icv treatment group with a final total of 7 (CCI + saline) or 8 (CCI + mithramycin) animals per group. At 24 h post-injury the animals were euthanized and the injured cortex was analyzed.

Experimental design and statistical analysis

For in vitro LDH, calcein, qPCR, and western blot assays, at least three separate wells of primary RCN seeded on day 0 from the same primary culture were used for any given assay. These separately cultured and treated neurons isolated from the same pool of embryos were run on the same gel/assay plate and quantified as indicated elsewhere. Each set of experiments (except ChIP) involving etoposide +/- mithramycin was repeated at least twice in an equivalent manner with another pool of embryos from a different pregnant dam and showed consistent results. Experiments with other cell death inducers besides etoposide were repeated at least once. For mitochondrial function analysis, each plate ($n = 4$) came from a separate pool of embryos, and each contained separately cultured and treated neurons (different wells, each seeded with the same number of neurons) isolated from the same pool of embryos.

All immunofluorescent analysis was done on multiple fields from a single coverslip for each treatment and each timepoint. These coverslips came from separately cultured and treated neurons (different wells) isolated from a single pool of embryos. The experiments were repeated as described in the paragraph above and showed consistent results.

Statistical analysis was performed using GraphPad Prism 8 (La Jolla, CA). For mitochondrial function tests, we used a one-way repeated-measures ANOVA with Tukey's post hoc tests. LDH, Calcein, ChIP, qPCR and western blot assays were all analyzed via one-way ANOVA with Tukey's post hoc tests. Immunocytochemically stained cells were analyzed using the Kruskal–Wallis test followed by Dunn's post hoc analysis for phospho-P53 and phospho-c-Jun (S73) and with one-way ANOVA with Tukey's post hoc tests for cleaved PARP and cleaved Casp3 analyses. All data analyzed with one-way ANOVA with Tukey's post hoc tests met the normality assumption by the Shapiro–Wilk test. Otherwise, the data were analyzed using the Kruskal–Wallis test, followed by Dunn's post hoc tests. When appropriate, we tested for unequal variance by the Brown–Forsythe test and if unequal, we utilized the Brown–Forsythe

ANOVA test followed by Dunnett's T3 multiple comparisons test.

Results

Mithramycin's neuroprotective effects are cell death model-specific

Etoposide (DNA-damage inducer; 50 μ M) treatment (24 h) resulted in significant rat cortical neuron (RCN) death, as shown by increased LDH release (indicator of dying cells) and decreased calcein signal (indicator of surviving cells) (Fig. 1a). Mithramycin co-treatment had significant, dose-dependent neuroprotective effects in both measures (Fig. 1a). We subsequently used 200 nM mithramycin, except when indicated.

To characterize mithramycin's long-term neuroprotective effects, RCN were treated for 24 h followed by media replacement with RCN-conditioned media (no etoposide or mithramycin) and further incubation until 48 or 72 h. RCN treated with etoposide showed increased cell death (higher LDH) and progressively decreased survival (lower calcein) at 24, 48, and 72 h after treatment (Fig. 1b). Decreased LDH signal levels vs. controls at 48 and 72 h are due to media replacement after 24 h. Mithramycin co-treatment had a long-term neuroprotective effect in both measures at all time points. Mithramycin alone resulted in a minor decrease in neuronal viability, especially at later time points (Fig. 1a, b).

We also examined mithramycin's neuroprotective effects in additional DNA-damage-dependent (camptothecin/doxorubicin) as well as DNA-damage-independent (staurosporine/ C_2 -ceramide) cell death models. Doxorubicin (200 nM) (Fig. 1c) or camptothecin (10 μ M) (Fig. 1d) caused significant RCN death by both LDH and calcein measures. Mithramycin co-treatment was neuroprotective at all tested doses.

Staurosporine (0.5 μ M) (Fig. 1e) or C_2 -ceramide (50 μ M) (Fig. 1f) caused RCN death by both LDH and calcein measures. Mithramycin co-treatment had a minor neuroprotective effect in the C_2 -ceramide model as indicated by the decrease in LDH release; no effect was detected on calcein signal. Interestingly, mithramycin co-treatment resulted in increased RCN cell death in the staurosporine model by both measures.

Mithramycin attenuates etoposide-induced apoptotic pathways downstream of p53 activation

Etoposide induced DNA-damage markers, phosphorylated ataxia-telangiectasia, mutated (ATM) (S1981) and phosphorylated H2A histone family member X (S139) (γ H₂AX) at all time points (western blot) (Fig. 2a). Co-treatment with mithramycin did not significantly change the levels of either marker, except a modest increase at later time points that may reflect increased neuronal survival (Fig. 2a). Lack of mithramycin effect on γ H₂AX

was also confirmed by immunocytochemistry (data not shown). Quantitative analysis of phospho-p53 immunocytochemistry and western blotting (Fig. 2a, b) indicated that etoposide increased levels of activated p53 [mean rank diff. = 355.6 in Fig. 2b]. Mithramycin co-treatment had no significant effects on etoposide-induced increases in phospho-p53 levels (western blot) (Fig. 2a) or population distribution (immunocytochemistry) (Fig. 2b).

Etoposide also resulted in elevations of pro-apoptotic molecules downstream of p53, including p53-upregulated mediator of apoptosis (PUMA) and cyclin-dependent kinase inhibitor 1 (cdkn1a/p21), that were significantly attenuated via mithramycin co-treatment (western blot) (Fig. 2a).

Etoposide-treated RCN showed increased execution-stage apoptosis markers including activated (cleaved fragment) caspase-3 and caspase-7 as well as increased cleavage of substrates, Fodrin (120 kDa) and PARP (89 kDa) (Fig. 2c). The increase in Fodrin's calpain/caspase-dependent cleavage fragments (145/150 kDa) was more modest. Mithramycin co-treatment significantly attenuated all described caspase activation markers/cleavage products as well as the etoposide-induced decrease in synaptic marker PSD95, a general indicator of neuronal degeneration/loss (Fig. 2c).

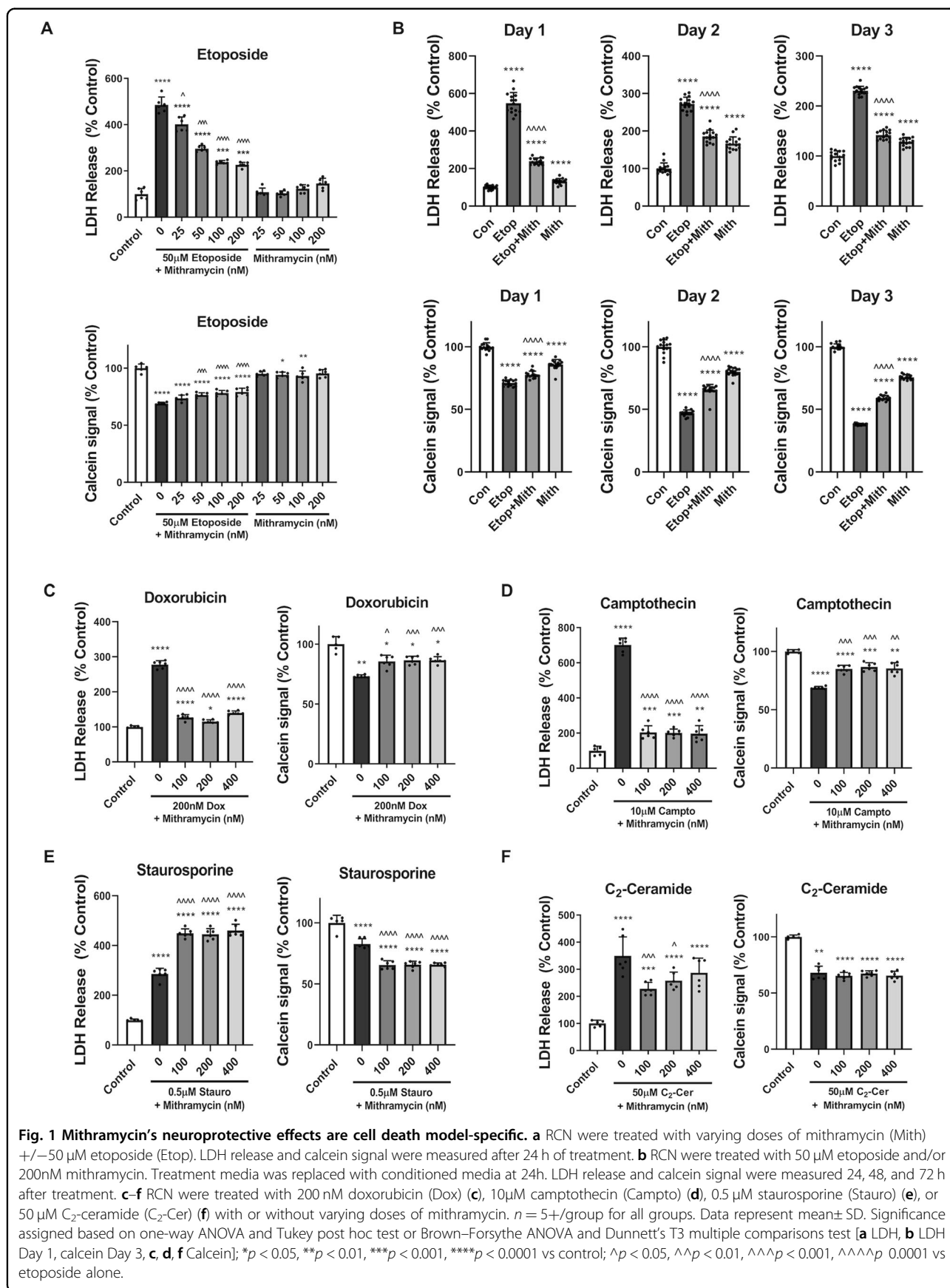
Mithramycin reduces etoposide-induced mitochondrial damage and attenuates p53-dependent transcription

Etoposide treatment of RCN caused early (6 h) mitochondrial outer membrane permeabilization (MOMP) as seen by cytosolic release of pro-apoptotic AIF and CytC (western blot) (Fig. 3a), while mithramycin co-treatment decreased release and thus showed preserved mitochondrial integrity (Fig. 3a). Standard normalizing proteins are degraded at late stages of apoptosis⁴⁶, and both actin (Fig. 3a) and GAPDH (data not shown) showed a decline at 24 h in purified cytoplasmic fractions.

Etoposide treatment (6 h) also caused mitochondrial functional decline, demonstrated by significant reductions in maximum and spare respiratory capacities (Seahorse Analyzer) that were rescued by mithramycin co-treatment (Fig. 3b). We have previously shown no significant neuronal loss at the etoposide 6 h timepoint³⁷.

Etoposide-treated RCN showed increased mRNA levels of PUMA, phorbol-12-myristate-13-acetate-induced protein 1 (Pmaip1/Noxa) and p21 (qPCR). These changes were substantially attenuated by Mithramycin co-treatment (Fig. 3d).

Chromatin Immunoprecipitation demonstrated that etoposide-treated RCN displayed increased Sp1- and p53 binding to the same Noxa promoter region vs. controls (Fig. 3e). Mithramycin co-treatment decreased only the Sp1 binding to this Noxa promoter region (Fig. 3e).



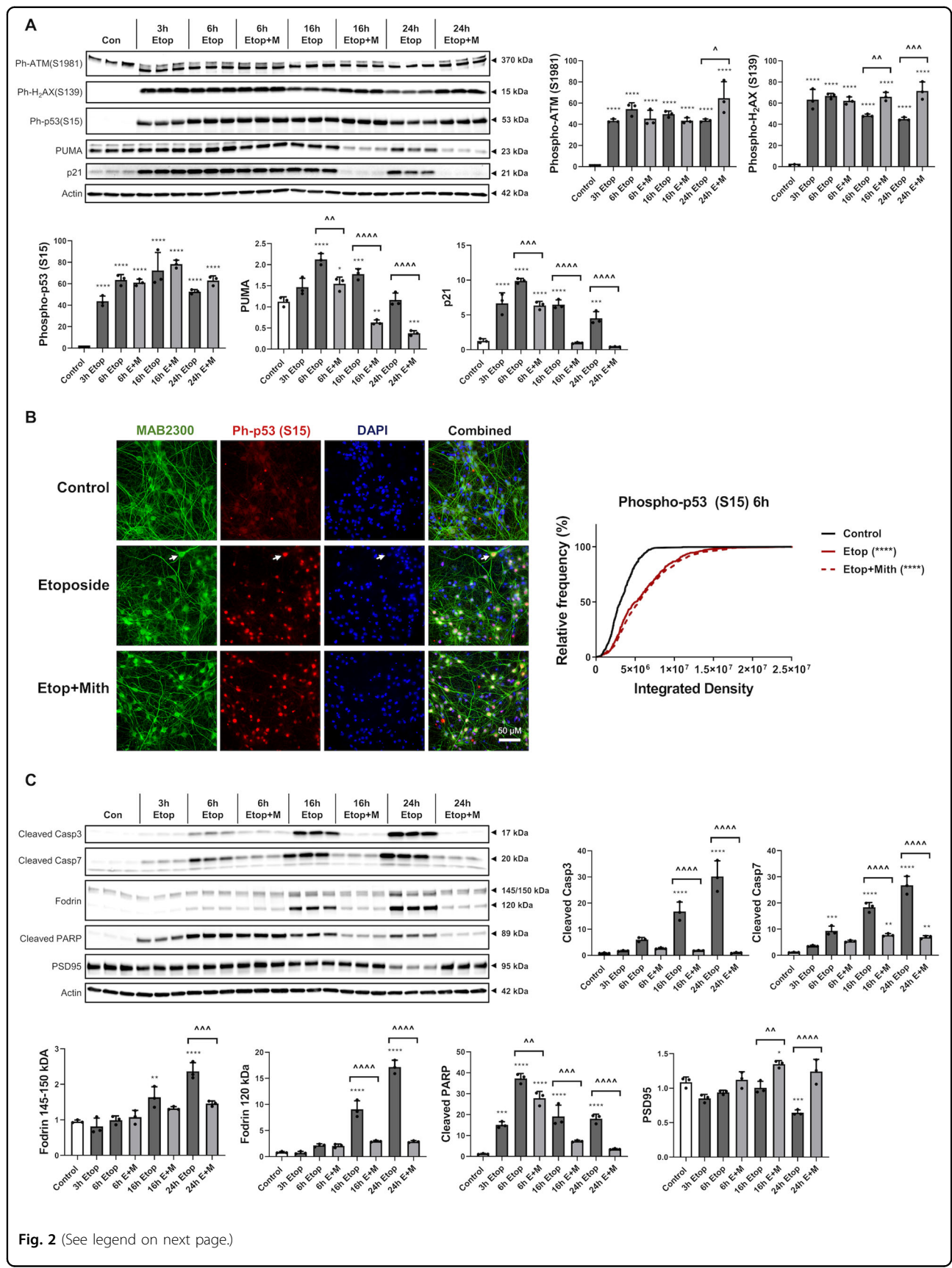


Fig. 2 (See legend on next page.)

(see figure on previous page)

Fig. 2 Mithramycin attenuates etoposide-induced apoptotic pathways downstream of p53 activation. **a, c** RCN were treated with 50 μ M etoposide +/-200 nM mithramycin. After 3, 6, 16, or 24 h, cells were harvested. Equal amounts of whole-cell lysates were loaded onto an SDS-polyacrylamide gel and after electrophoretic separation and transfer to a membrane were incubated with antibodies against DNA-damage markers: phospho-ATM (S1981) and γ H₂AX, or phospho-p53 (S15) and its downstream targets: PUMA and p21 (**a**). Other membranes were incubated with antibodies against cleaved/activated caspase-3 (Casp3) and caspase-7 (Casp7), their substrates α -Fodrin and cleaved PARP, as well as PSD95 (**c**). Protein levels (of bands indicated by arrows) were quantified by densitometry, normalized to appropriate β -actin signal and are presented as normalized fold change compared with control levels. Representative actin blots are shown here. $n = 3$ /group for all groups. Data represent mean \pm SD. Significance assigned based on one-way ANOVA and Tukey post hoc test; * $p < 0.05$, ** $p < 0.01$, *** $p < 0.001$, **** $p < 0.0001$ vs control; $\wedge p < 0.05$, $\wedge\wedge p < 0.01$, $\wedge\wedge\wedge p < 0.001$, $\wedge\wedge\wedge\wedge p < 0.0001$ vs etoposide alone. **b** Phospho-p53 (S15) levels were also analyzed by immunocytochemistry after 6 h. A representative set of $\times 63$ images is shown here, white arrows indicate sample neuron co-localized with ph-p53 (S15). Quantification of cells was done across at least 6 fields per treatment. Data are presented as an unbinned cumulative frequency distribution. Significance assigned based on Kruskal–Wallis test followed by Dunn’s post hoc analysis; **** $p < 0.0001$ vs control.

Etoposide increased Sp1 mRNA levels and mithramycin co-treatment attenuated these changes, likely because Sp1 activates its own transcription⁴⁷. Protein levels of Sp1 show a divergent profile with an etoposide-induced decrease, likely due to early apoptotic degradation⁴⁸, partially rescued by mithramycin co-treatment. Therefore, mithramycin’s effects are not driven by Sp1 protein loss (Fig. 3f).

Although etoposide decreased the levels of pro-survival miR-23a³⁵ and increased levels of pro-apoptotic miR-711⁴⁹ while decreasing the level of its target mRNAs^{36,49} vs. control, mithramycin co-treatment had no effect on these changes (qPCR) except a late (24 h) increase in Akt mRNA (Fig. 3g, h).

Mithramycin attenuates etoposide-induced activation of the c-Jun injury response

RCN treated with etoposide showed c-Jun activation, including significantly increased levels of phospho-c-Jun (Ser63), phospho-c-Jun (Ser73) and total c-Jun (western blot) (Fig. 4a). Etoposide treatment also increased c-Fos protein levels. Mithramycin co-treatment significantly reduced all four markers (western blot) (Fig. 4a). Multiple close c-Jun bands suggest extensive post-translational modification, including phosphorylation, causing gel mobility shifts. In addition, the c-Jun antibody recognizes both a 43 kDa and 48 kDa form. In *in vitro* samples, we quantified these bands together as they were both present and regulated in parallel.

Quantitative analysis of phospho-c-Jun (S73) immunocytochemistry showed a progressive increase in signal intensity of phospho-c-Jun (S73)-positive neurons in etoposide-treated RCN (Fig. 6b). Mithramycin co-treatment reduced these changes, pushing the population distribution curve to the left (Fig. 4b), with a mean rank difference that progressively increased and was 288 at 6 h, 1227 at 12 h, and 2163 at 24 h (Fig. 4b).

Etoposide increased c-Jun mRNA levels (6 and 24 h); these changes were attenuated by mithramycin co-treatment to below control levels (Fig. 4c).

Mithramycin’s attenuation of apoptotic mechanisms in neurons is cell death model-specific

To determine the range of mithramycin’s effects we examined its activity in various neuronal apoptosis models. Doxorubicin caused an early (6 h) and sustained (24 h) increased activation of DNA-damage responses including elevation of both phospho-ATM and γ H₂AX (western blot) (Fig. 5). In contrast, C₂-ceramide and staurosporine did not significantly change phospho-ATM levels. Similarly, C₂-ceramide had no effect on γ H₂AX levels while staurosporine only modestly increased γ H₂AX (Fig. 5). Mithramycin co-treatment robustly attenuated doxorubicin-induced phospho-ATM but only modestly attenuated γ H₂AX levels. Mithramycin co-treatment did not change phospho-ATM levels after C₂-ceramide and staurosporine treatment and led to increased γ H₂AX levels. This latter effect was substantial after staurosporine 24 h treatment (Fig. 5).

Doxorubicin was the only inducer to significantly increase phospho-p53 (S15) levels and elevate PUMA and p21. Mithramycin co-treatment attenuated the doxorubicin-mediated changes downstream of phospho-p53 (S15). Consistent with changes observed in the etoposide model (Fig. 2), PUMA levels were lower in mithramycin co-treated samples in all three models (Fig. 5).

All three cell death models led to progressive caspase pathway activation, including early (6 h) elevation in cleaved Casp3 as well as increased caspase-dependent cleavage fragments of Fodrin (120 kDa) and PARP (89 kDa); these changes were further amplified at 24 h (western blot) (Fig. 5). The increase in the calpain/caspase-dependent cleavage fragments of Fodrin (145/150 kDa) was more modest. Mithramycin co-treatment consistently attenuated the doxorubicin and C₂-ceramide caspase-dependent apoptotic markers but only temporarily (6 h) reduced several staurosporine-dependent changes, as well as causing an increase in staurosporine-dependent changes at 24 h. Consistent with the results of viability experiments (Fig. 1), mithramycin co-treatment

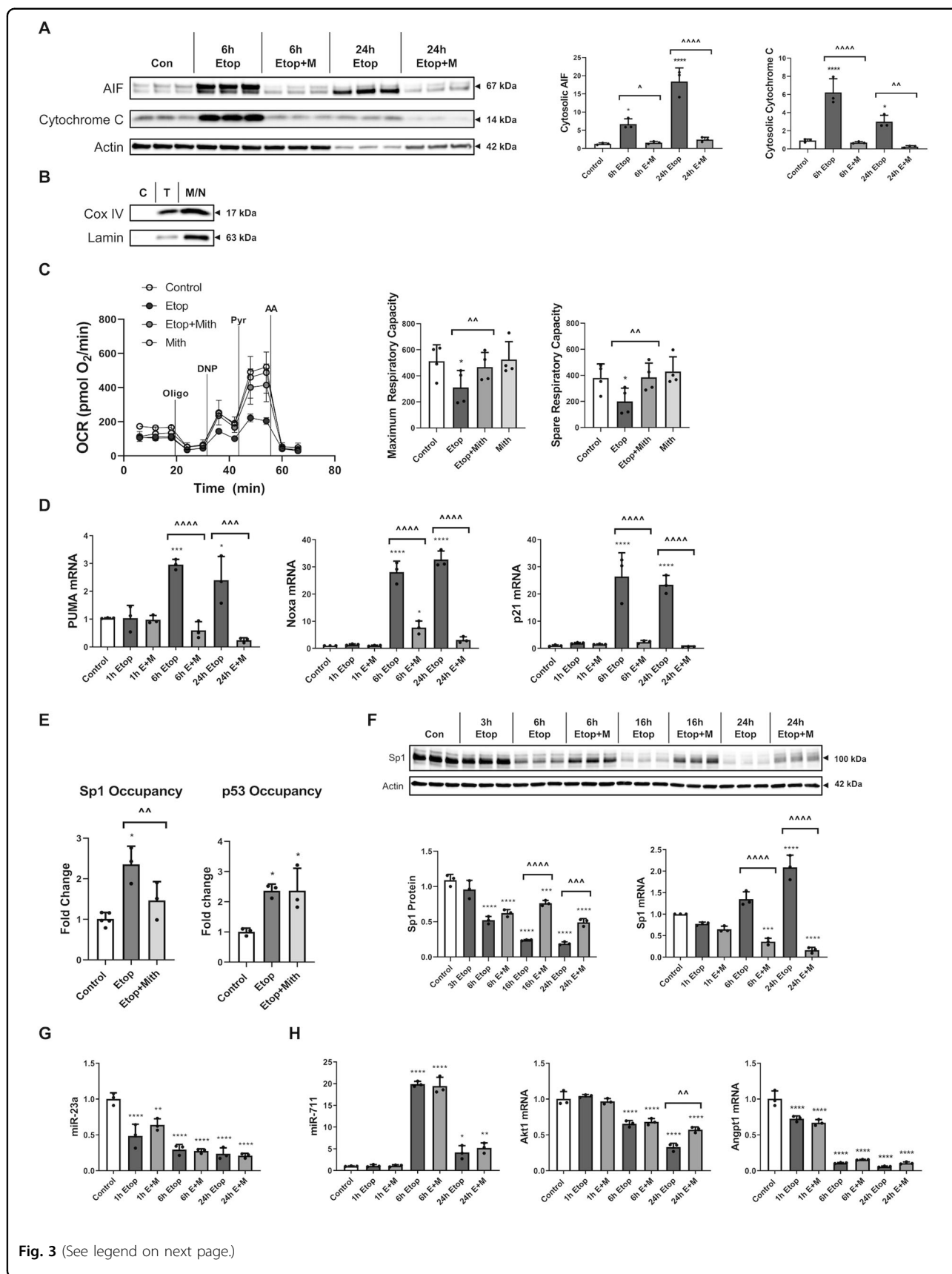


Fig. 3 (See legend on next page.)

(see figure on previous page)

Fig. 3 Mithramycin reduces etoposide-induced mitochondrial damage and attenuates p53-dependent transcription. RCNs were treated with 50 μ M etoposide \pm 200 nM Mithramycin for all panels. **a** The cytosolic fraction was collected after 6h and 24 h. Controls were collected at 24h. Equal amounts of fraction lysates were loaded onto an SDS-polyacrylamide gel and after electrophoretic separation and transfer to a membrane were incubated with antibodies against AIF and cytochrome C proteins. Protein levels (of bands indicated by arrows) were quantified by densitometry, normalized to β -actin signal and are presented as normalized fold change compared with control levels. $n = 3$ /group for all groups. **b** Cytoplasmic (C), total (T), and nuclear/mitochondrial (N/M) fractions were pooled and probed for cytochrome c oxidase IV (COX IV) and Lamin to confirm purity of cytoplasmic fraction from mitochondria and nuclei, respectively. **c** 6h after treatments, cellular respiration was measured using a Seahorse XF24 Extracellular Flux Analyzer, and a representative measurement is shown here. Sequential addition of oligomycin, DNP, pyruvate and antimycin A was utilized to identify maximum and spare respiratory capacity (**c**). Each group contains $n = 4$ averages from separate experiments on different days, each experiment except one contained $n = 4+$ separately cultured wells of neurons per group (that experiment contained wells that were eliminated due to no significant increase in OCR over baseline indicating a failed injection/port, $n = 3+$ /group for that experiment). **d, f–h** After 1, 6, or 24h, cells were harvested. Equal amounts of purified RNA were converted into cDNA. Equal volumes of cDNA were loaded for qPCR. mRNA/miRNA levels were normalized via U6/GAPDH (respectively), quantified using the ddCt method and are presented as fold change compared with control levels. $n = 3$ /group for all groups. **e** Chromatin Immunoprecipitation was done using p53 or Sp1 antibodies, and equal volumes of resulting DNA fragments were loaded for qPCR. Pulled-down DNA levels were normalized using ChIP Inputs, quantified using the 2^{-ddCt} method and are presented as fold change compared with control levels. **f** Electrophoresis and western blotting were performed for Sp1 protein. Protein levels were quantified by densitometry, normalized to β -actin signal and are presented as normalized fold change compared with control levels. $n = 3$ /group for all groups. Data all represent mean \pm SD. Significance assigned based on one-way ANOVA and Tukey post hoc test; * $p < 0.05$, ** $p < 0.01$, *** $p < 0.001$, **** $p < 0.0001$ vs control; $\wedge p < 0.05$, $\wedge\wedge p < 0.01$, $\wedge\wedge\wedge p < 0.001$, $\wedge\wedge\wedge\wedge p < 0.0001$ vs etoposide alone.

attenuated the loss of neuronal marker PSD95 only in the doxorubicin paradigm and even accentuated late (24 h) PSD95 decline in the staurosporine model (Fig. 5).

We performed quantitative immunocytochemical analyses of activated caspase-3 and cleaved PARP at an early (6 h) time point to detect mithramycin-induced changes that mark the beginning of the execution phase of caspase-dependent neuronal death. Etoposide and doxorubicin led to significant increases in the number/intensity of cleaved caspase-3- and cleaved PARP-positive neurons while mithramycin co-treatment significantly attenuated these changes (Fig. 6). Consistent with western blot data (Fig. 5), C_2 -ceramide resulted in only modest changes. Staurosporine led to more substantial caspase-3 activation and PARP cleavage than C_2 -ceramide but these were not decreased by mithramycin co-treatment (Fig. 6).

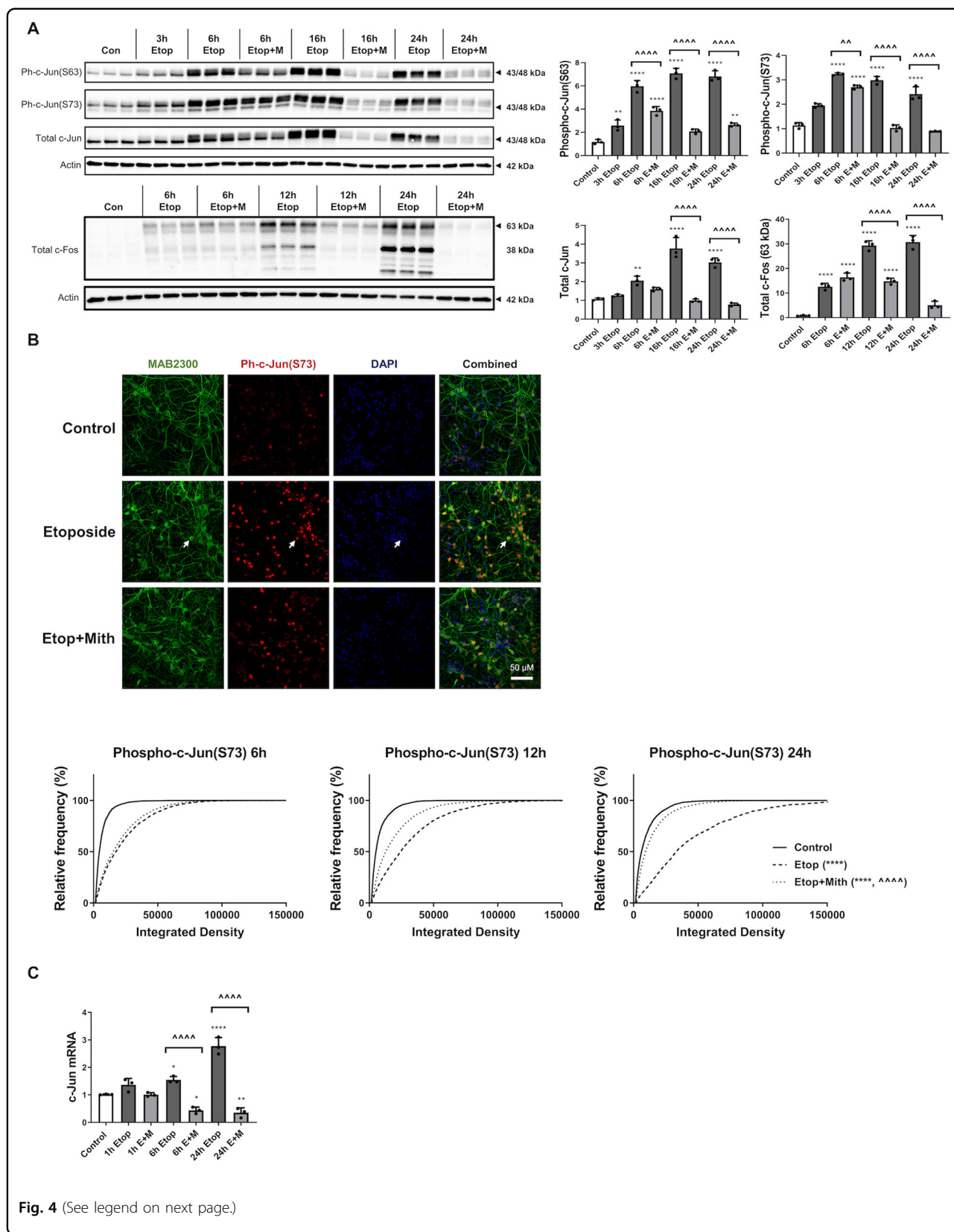
Mithramycin's attenuation of the c-Jun injury response in neurons is cell death paradigm-specific

We analyzed markers of c-Jun activation in various RCN apoptotic models using western blot for phospho-c-Jun (S73) and phospho-c-Jun (S63) and immunocytochemistry for phospho-c-Jun (S73). C_2 -ceramide resulted in rapid (6 h) c-Jun phosphorylation which remained at a high, albeit lowered, level at 24 h (western blot) (Fig. 7). Co-treatment with mithramycin robustly attenuated these changes. Doxorubicin caused only modest c-Jun activation at 6 h (S63) while staurosporine showed a late activation at 24 h (S63 and S73) (Fig. 7). Mithramycin co-treatment attenuated the latter changes. We used quantitative immunocytochemical analysis of phospho-c-Jun (S73) to characterize early-stage (6 h) neuronal c-Jun activation at single-cell resolution. We found that

etoposide [mean rank diff. = 1339], C_2 -ceramide [mean rank diff. = 1213] and, to a far lesser extent, doxorubicin [mean rank diff. = 793.7] showed an increase in signal intensity of phospho-c-Jun (S73)-positive cells at 6 h, corresponding to a rightward shift of the population curve (Fig. 7). Mithramycin co-treatment attenuated staining intensity only in the etoposide group [mean rank diff. = 393.9], and had no significant overall effect on the doxorubicin group, possibly because the effect size of doxorubicin alone was very small, or on the C_2 -ceramide group, although it appeared to shift the distribution to the left but only in the range of the highest phospho-c-Jun (S73)-expressing cells (Fig. 7).

Mithramycin treatment attenuates neuronal death pathways after experimental TBI in vivo

We examined the effects of mithramycin (icv administration) on neuronal cell death pathways' activation 24 h after controlled cortical impact (CCI). CCI + Veh showed increased cortical levels of phospho-H2AX (S139), phospho-P53 (S15), p21, cleaved caspase-3, and Fodrin (145/150 kDa) compared with Sham. Mithramycin treatment significantly decreased levels of Fodrin cleavage (145/150 kDa and 120 kDa) compared with CCI + Veh. Although other markers' mean values indicate mithramycin-induced attenuation of the injury-induced upregulation, these changes did not reach statistical significance due to the modest degree of the change and/or biological variability. Nonetheless, the absence of significant differences in cleaved caspase-3 between CCI + Mith and Sham groups suggests a mithramycin-dependent attenuation of injury upregulation of active caspase-3 (Fig. 8a). To comparably quantify effective caspase activity across models/treatments we defined the



(see figure on previous page)

Fig. 4 Mithramycin attenuates etoposide-induced activation of the c-Jun injury response. RCN were treated with 50 μ M etoposide +/-200 nM mithramycin for all panels. **a** After 3, 6, 12, 16, or 24 h, cells were harvested. Equal amounts of whole-cell lysates were loaded onto an SDS-polyacrylamide gel and after electrophoretic separation and transfer to a membrane were incubated with antibodies against phospho-c-Jun (S63), phospho-c-Jun (S73), total c-Jun, and total c-Fos proteins. Protein levels (of bands indicated by arrows) were quantified by densitometry, normalized to appropriate β -actin signal and are presented as normalized fold change compared with control levels. Representative actin blot is shown here. $n = 3$ /groups for all groups. Data all represent mean \pm SD. Significance assigned based on one-way ANOVA and Tukey post hoc test; ** $p < 0.01$, **** $p < 0.0001$ vs control; ^^ $p < 0.01$, ^^ $p < 0.0001$ vs etoposide alone. **b** RCN were fixed with formaldehyde 6, 12, or 24h after treatment and stained with antibodies for neuronal markers (MAB2300, Neuro-Chrom™ Pan-Neuronal Marker), ph-c-Jun (S73), and DAPI for fluorescent imaging. Representative images are from $\times 63$ magnification at 12 h, white arrows indicate sample neuron co-localized with ph-c-Jun (S73). At least four fields at $\times 20$ magnification were quantified for each treatment as described in materials and methods. Data were graphed as an unbinned cumulative frequency distribution. Using Kruskal–Wallis test, followed by Dunn’s post hoc analysis, all groups at all time points had significantly different distributions, **** $p < 0.0001$ vs control, ^^ $p < 0.0001$ vs etoposide alone. **c** After 1, 6, or 24h, cells were harvested. Equal amounts of purified RNA were converted into cDNA. Equal volumes of cDNA were loaded for qPCR. mRNA levels were normalized via GAPDH, quantified using the 2^{-ddCt} method and are presented as fold change compared with control levels. $n = 3$ /group for all groups. Data all represent mean \pm SD. Significance assigned based on one-way ANOVA and Tukey post hoc test; * $p < 0.05$, ** $p < 0.01$, **** $p < 0.0001$ vs control; ^^ $p < 0.0001$ vs etoposide alone.

“Caspase Activity Index” based on substrate cleavage, as the ratio of 120 kDa/145–150 kDa Fodrin bands’ intensity. It inverted from a higher numerator in in vitro models, indicative of strong caspase activation, to a higher denominator after mithramycin co-treatment in vitro and after TBI in vivo. Mithramycin had no additional effect in vivo (Fig. 8b).

CCI + Veh also resulted in increased cortical levels of phospho-c-Jun (S63), phospho-c-Jun (S73), and total c-Jun compared with Sham mice. As the expected 48 kDa band of phospho-c-Jun (S63) was masked by a non-specific band, we separately quantified each c-Jun band. Mithramycin treatment significantly decreased phospho-c-Jun (S63 and S73, 43 kDa band) levels vs. vehicle; reductions in phospho-c-Jun(S73)’s 48 kDa band and total c-Jun did not reach significance (Fig. 8a).

CCI + vehicle administration also led to increases in cortical PUMA and Noxa mRNA (Fig. 8c). Mithramycin treatment did not significantly decrease either mRNA’s levels, although absence of significant differences in Puma between CCI + Mith and Sham may suggest a mithramycin-dependent attenuation of injury upregulation of PUMA.

Discussion

Etoposide is a topoisomerase-II inhibitor that sequentially causes DNA strand breaks, p53 activation and intrinsic neuronal apoptosis^{37,49,50}. Mithramycin reduced etoposide-induced neuronal death and improved long-term survival, suggesting that mithramycin causes a sustained transformation in the pattern/progression of apoptotic processes rather than a temporary delay.

Mithramycin was also neuroprotective in other DNA-damage models including exposure to camptothecin, a topoisomerase-I inhibitor⁵¹, or doxorubicin, a topoisomerase-II inhibitor, DNA intercalator and widely used chemotherapy agent⁵². In contrast, mithramycin was ineffective in

staurosporine⁵³ or C₂-ceramide⁵⁴ models of neuronal apoptosis, which are DNA-damage-independent^{53,55}. Thus, mithramycin may preferentially target DNA-damage-dependent neuronal cell death pathways and its neuroprotective effects^{30,33,56} may be restricted to conditions where these mechanisms dominate.

Phosphorylation/activation of ATM is an early DNA-damage response, which serves to phosphorylate H₂AX and initiate DNA repair pathways⁵⁷ but may also activate kinases that stimulate p53 and downstream apoptosis pathways⁵⁸. The balance between restorative and cell death programs determines neuronal fate after DNA damage⁵⁹. Mithramycin neither inhibited etoposide-induced ATM and H₂AX phosphorylation, nor reduced p53 phosphorylation, indicating that it does not directly affect early DNA damage/repair processes or p53 activation, but acts on downstream or independent apoptotic pathways. Mithramycin strongly attenuated etoposide-induced caspase-3/7 activation and decreased caspase substrate cleavage (PARP and Fodrin). The irreversible proteolytic cleavage of these substrates is a marker of entry into the execution phase of apoptosis, the end-stage for dying neurons⁶⁰, while its attenuation is an oft-used marker of neuroprotection^{61–63}. Upstream of caspase activation, MOMP has been identified as a critical and irreversible step in the intrinsic apoptosis pathway⁶⁴. Etoposide treatment induced early (6 h) elevated cytosolic levels of AIF/CytC and a decline in mitochondrial respiration capacity/bioenergetic function; mithramycin attenuated these changes. Our results, confirmed in the doxorubicin model, indicate that mithramycin acts upstream of MOMP and caspase activation to protect neurons following DNA damage.

Phospho-p53 (S15) transactivates promoters of pro-apoptotic Bcl-2 family members leading to MOMP and apoptosis^{65–67}. Mithramycin attenuated etoposide- and doxorubicin-mediated induction of key pro-apoptotic

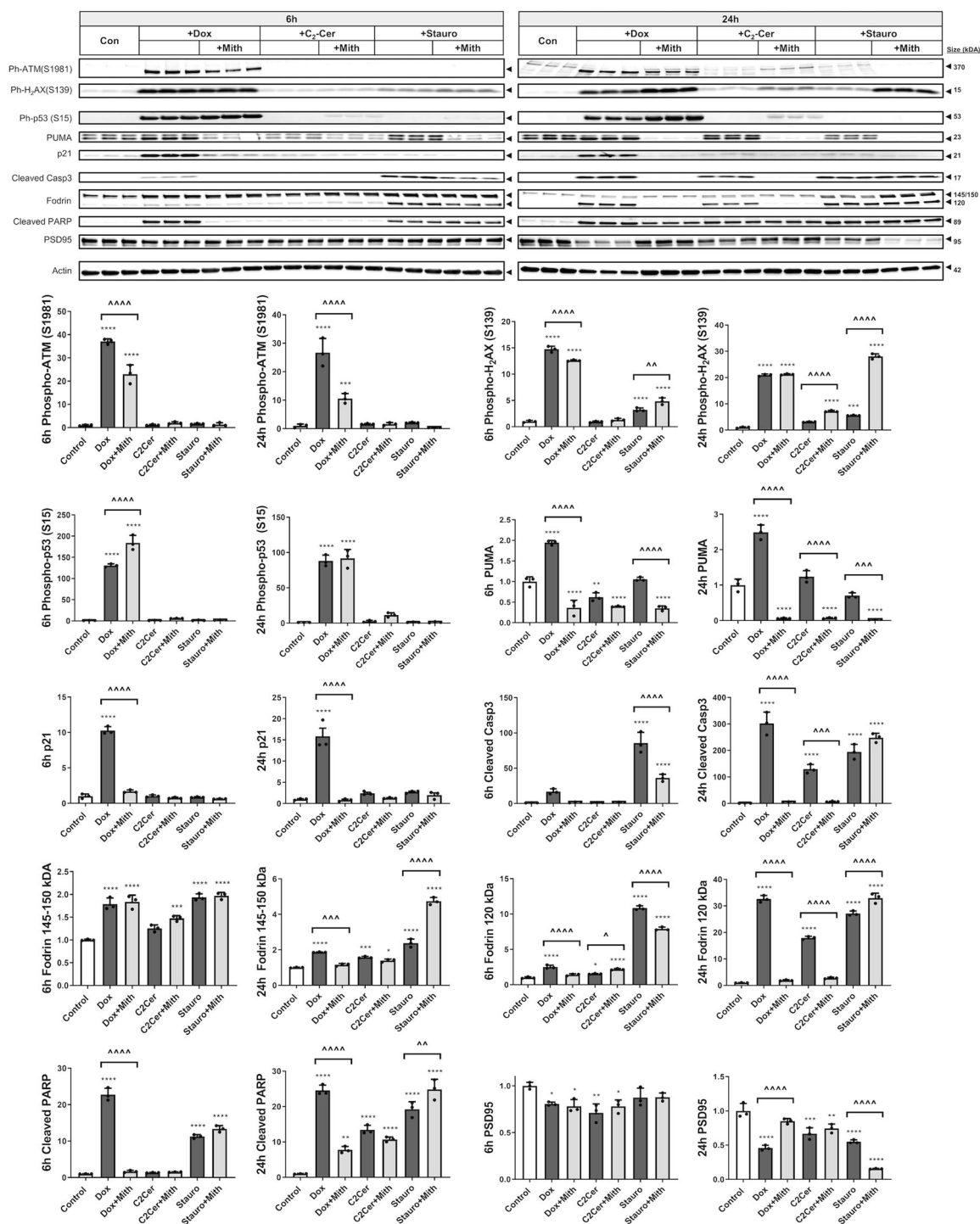


Fig. 5 Mithramycin's attenuation of apoptotic mechanisms in neurons is cell death model-specific. RCN were treated with 200 nM doxorubicin, 50 μM C₂-ceramide, or 0.5 μM staurosporine +/- 200 nM mithramycin. After 6 or 24 h, cells were harvested, equal amounts of whole-cell lysates were loaded onto an SDS-polyacrylamide gel and after electrophoretic separation and transfer to a membrane were incubated with antibodies against DNA-damage markers, phospho-p53 (S15) and its downstream proteins, PUMA and p21, as well as active caspase-3, its targets, PARP and Fodrin, and the synaptic marker PSD95. Protein levels (of bands indicated by arrows) were quantified by densitometry, normalized to β-actin signal and are presented as fold change compared with control levels. *n* = 3/groups for all groups. Data all represent mean ± SD. Significance assigned based on one-way ANOVA and Tukey post hoc test; **p* < 0.05, ***p* < 0.01, ****p* < 0.001, *****p* < 0.0001 vs control; ^*p* < 0.05, ^^*p* < 0.01, ^^*p* < 0.001, ^^*p* < 0.0001 vs cell death inducer alone.

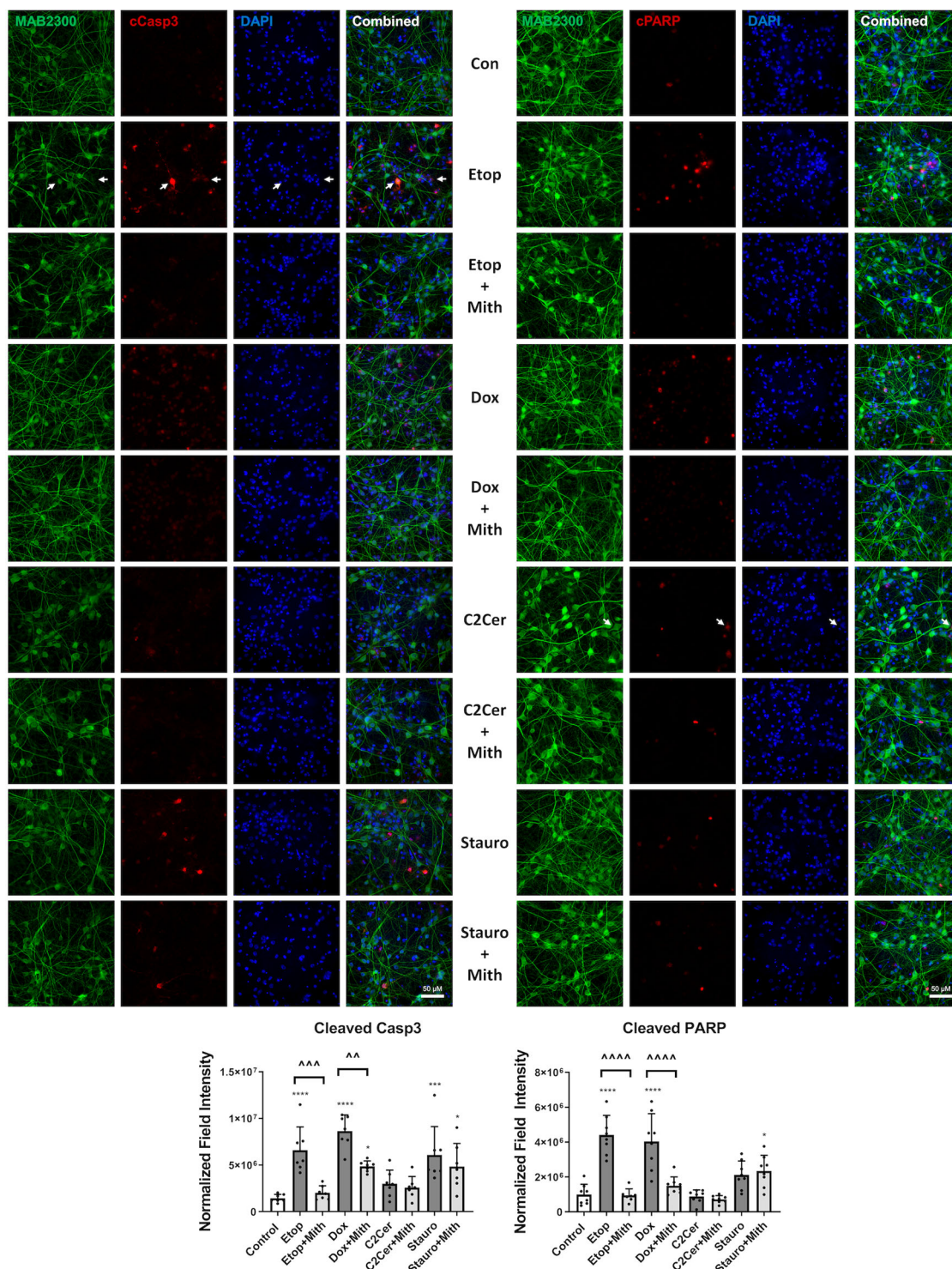
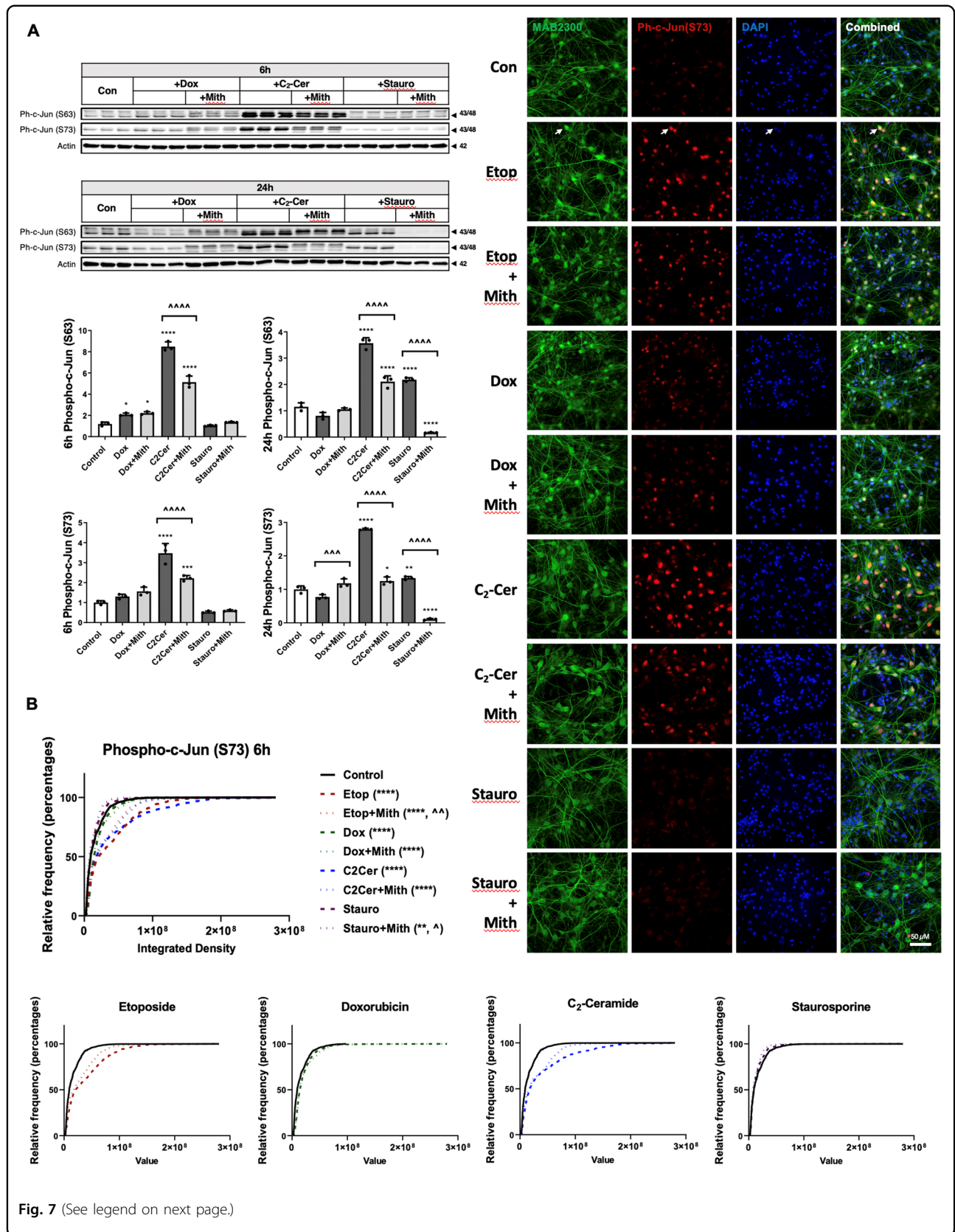


Fig. 6 Mithramycin’s effect on immunofluorescent markers of caspase activation in neurons is cell death model-specific. RCN were treated with 200 nM doxorubicin, 50 μM etoposide, 50 μM C₂-ceramide, or 0.5 μM staurosporine +/-200 nM mithramycin. After 6 h, cells were fixed and stained for neuronal markers (MAB2300, Neuro-Chrom™ Pan-Neuronal Marker), DAPI and cleaved Casp3 or cleaved PARP, imaged, and quantified. A representative field for each image at 63x magnification is shown. The Milli-Mark™ Pan-Neuronal Marker is not able to successfully stain those neurons who are close to the end stages of cell death (caspase activation); however, white arrows indicate cleaved Casp3/cleaved PARP cells that show a clear neuronal morphology. Quantification was performed on at least seven fields for each treatment. Data all represent mean ± SD. Significance assigned based on one-way ANOVA and Tukey post hoc test; **p* < 0.05, ****p* < 0.001, *****p* < 0.0001 vs control; ^^*p* < 0.01, ^^*p* < 0.001, ^^*p* < 0.0001 vs cell death inducer alone.



(see figure on previous page)

Fig. 7 Mithramycin's attenuation of the c-Jun injury response in neurons is cell death paradigm-specific. **a** RCN were treated with 200nM doxorubicin, 50 μ M C₂-ceramide, or 0.5 μ M staurosporine +/-200 nM mithramycin. After 6 h or 24 h, cells were harvested, equal amounts of whole-cell lysates were loaded onto an SDS-polyacrylamide gel and after electrophoretic separation and transfer to a membrane were incubated with antibodies against phospho-c-Jun (S63) and phospho-c-Jun (S73). Protein levels (of bands indicated by arrows) were quantified by densitometry, normalized to appropriate β -actin signal and are presented as normalized fold change compared with control levels. Representative actin blots are shown here. $n = 3$ /groups for all groups. Data all represent mean \pm SD. Significance assigned based on one-way ANOVA and Tukey post hoc test; * $p < 0.05$, ** $p < 0.01$, *** $p < 0.001$, **** $p < 0.0001$ vs control; ^^ $p < 0.001$, ^^ $p < 0.0001$ vs cell death inducer alone. **b** RCN were treated with 200nM doxorubicin, 50 μ M etoposide, 50 μ M C₂-ceramide or 0.5 μ M staurosporine +/-200 nM mithramycin. After 6h, cells were fixed and stained for neuronal markers (MAB2300, Neuro-Chrom™ Pan-Neuronal Marker), DAPI and phospho-c-Jun (S73), imaged and quantified. A representative field for each image is shown, white arrows indicate an example of a neuron co-localized with ph-c-Jun (S73). Quantification was performed on at least eight fields per treatment and is plotted as an unbinned cumulative frequency distribution. Significance assigned based on Kruskal–Wallis test and Dunn's post hoc analysis; ** $p < 0.01$, **** $p < 0.0001$ vs control; $\wedge p < 0.05$, $\wedge\wedge p < 0.01$ vs cell death inducer alone.

Bcl-2 family members, BH3-only molecules Puma and Noxa, as well as p21, a cell death modulator and well-known p53 target molecule⁶⁷, despite no changes in p53 phosphorylation. Thus, Mithramycin regulates p53 pro-apoptotic transcriptional activity downstream of p53 phosphorylation across DNA-damage-dependent neuronal death models. Although we show broad Mithramycin-mediated down-regulation of injury markers, this is unlikely to be the result of a global non-specific decrease in transcription as mithramycin rescues levels of other mRNAs and proteins (e.g., PSD95) from etoposide-induced decline.

We have previously shown that miR-23a can target PUMA and Noxa mRNAs³⁵. However, mithramycin did not attenuate the rapid etoposide-dependent miR-23a decline, indicating that its effects on Puma and Noxa are miR-23a-independent. Similarly, miR-711 is a pro-apoptotic microRNA induced by etoposide that targets the pro-survival molecules Ang-1 or Akt⁴⁹ and can affect levels of Bcl-2 family members. As mithramycin co-treatment had no significant impact on these targets, except a late effect on Akt mRNA, Sp1 inhibition is unlikely to attenuate neuronal cell death by modulating the miR-711/PI3K/Akt pathway.

Sp1 has been shown to broadly alter p53's ability to transactivate promoters and facilitate apoptosis induction^{26,27,68}. Moreover, p53 and Sp family members interact in apoptotic gene regulation, and in some cell types, Sp1 is necessary for p53-mediated transcription of Bax and Puma, two Bcl-2 family members essential for p53-dependent apoptosis^{28,69}. In our primary neuron ChIP experiments, Mithramycin inhibited Sp1 promoter binding without changing p53 binding to the same Noxa promoter region. Thus, our data show that mithramycin affects neither p53 phosphorylation nor its recruitment to promoter sites and provide evidence that Sp1 is necessary for p53-mediated transcription of key pro-apoptotic molecules in DNA-damage-induced neuronal apoptosis, potentially by cooperating with p53 to transactivate pro-apoptotic gene promoters.

Unlike in DNA-damage-dependent models, we observed neither significant activation of p53-dependent apoptotic pathways, including p53 phosphorylation and BH3-only molecules' induction, nor strong mithramycin neuroprotection in DNA-damage-independent models. Nonetheless, both C₂-ceramide and staurosporine paradigms display robust caspase-3 substrate cleavage, suggesting that caspase pathway activation in those paradigms is significantly p53/BH3-independent. The involvement of model-specific neuronal death mechanisms is further evidenced by mithramycin-dependent attenuation of caspase activation after C₂-ceramide but not after staurosporine. However, caspase activation does not appear necessary for C₂-ceramide-induced neuronal death as mithramycin only modestly reduced the latter.

In concert with these changes in the canonical intrinsic apoptosis pathway, we also showed that mithramycin reduces etoposide-induced increases in protein levels of c-Jun (total and phosphorylated) and c-Fos as well as c-Jun mRNA levels. Modulation of c-Jun expression by mithramycin is likely due to the Sp1 sites present in the c-Jun promoter. Together, c-Jun and c-Fos dimerize to form the transcription factor AP-1⁷⁰, which can cooperate with p53 and Sp1 to affect many genes, including pro-apoptotic Bcl-2 family members^{71,72}. Our data therefore suggest that Sp1 modulation may affect two separate transcriptional pathways (p53 and AP-1) involved in neuronal cell death⁷³. Moreover, as Sp1 has also been shown to cooperate with c-Jun to activate gene transcription^{72,74}, mithramycin neuroprotective effects may also be due to directly modulating Jun-dependent transcription.

Although we show that induction of c-Jun pathways is a general neuronal injury response, its magnitude differs across models. Interestingly, it appears much weaker in doxorubicin vs. etoposide suggesting lack of uniform regulation even within DNA-damage models. In contrast, it is highly and rapidly upregulated by C₂-ceramide, where mithramycin's ability to suppress c-Jun levels supports a p53-independent mechanism. Despite the potential to

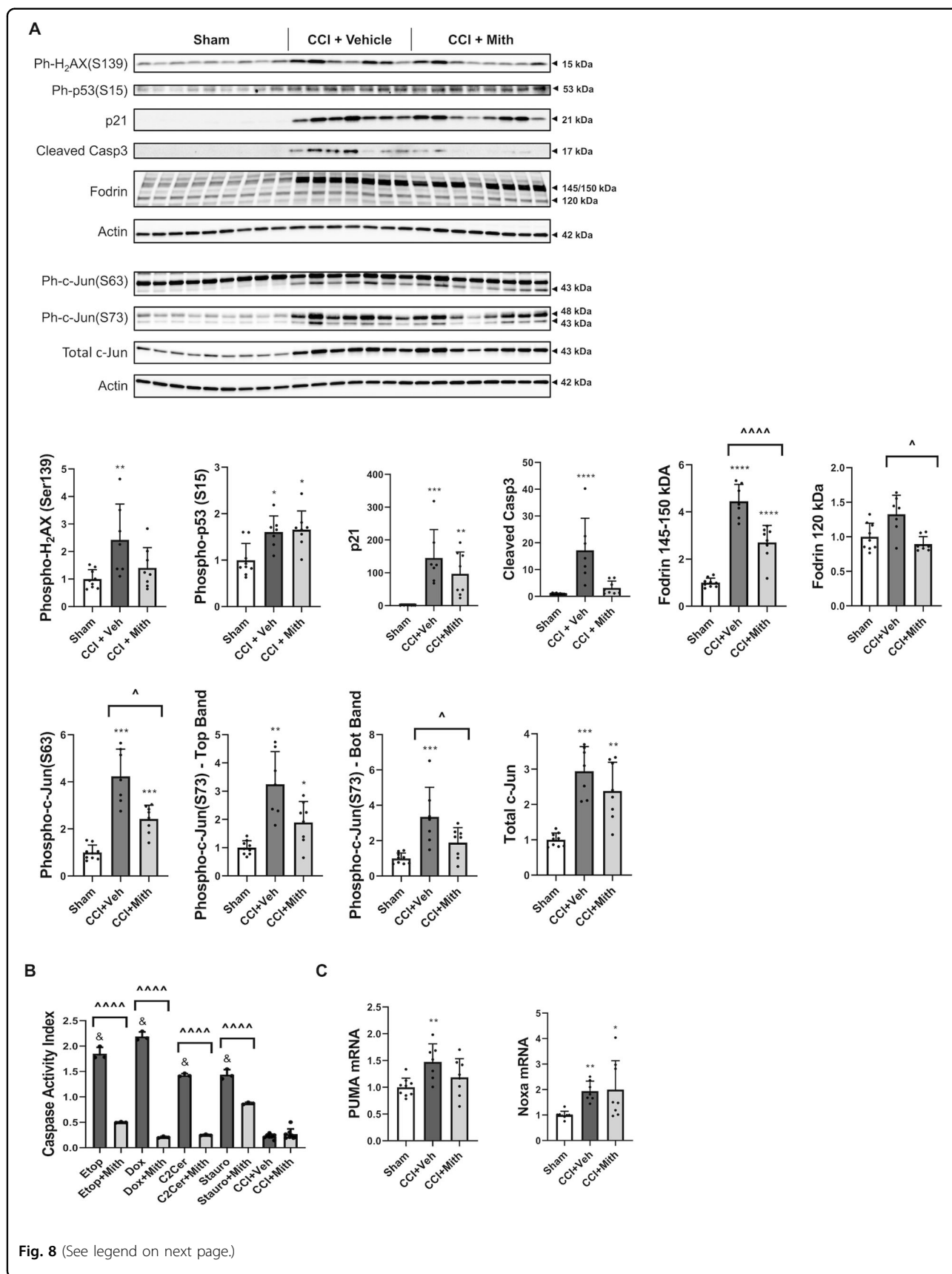


Fig. 8 (See legend on next page.)

(see figure on previous page)

Fig. 8 Mithramycin treatment attenuates neuronal death pathways after experimental TBI in vivo. **a** Whole-tissue lysates were obtained from ipsilateral-to-injury cortices 24 h after CCI+ intracerebroventricular injection of aCSF or mithramycin and from cortices of sham-injured animals. Equal amounts of whole-cell lysates were loaded onto an SDS-polyacrylamide gel and after electrophoretic separation and transfer to a membrane were incubated with antibodies against phospho-H₂AX (S139), phospho-p53 (S15), p21, cleaved caspase-3, and Fodrin as well as against phospho-c-Jun (S63), phospho-c-Jun(S73), total c-Jun proteins. Protein levels (of bands indicated by arrows) were quantified by densitometry, normalized to appropriate β -actin signal and are presented as normalized fold change compared with sham-injured animals. Representative actin blots are shown here. **b** The Caspase Activity Index, or proportion of 120kDa to 145–150kDa Fodrin fragments was calculated for each cell death inducer or CCI +/- mithramycin at 24h. $^8p < 0.0001$ vs. CCI + Veh. **c** RNA was purified from the cortex and converted into cDNA. Equal volumes of cDNA were loaded for qPCR. mRNA levels were normalized via GAPDH, quantified using the 2^{-ddCt} method and are presented as fold change compared with control levels. $n = 7$ +/group for all groups. Data represent mean \pm SD. Significance assigned based on one-way ANOVA and Tukey post hoc test, Brown–Forsythe ANOVA test followed by Dunnett’s T3 multiple comparisons test [ph-c-Jun (S63), ph-c-Jun (S73)-top band, total c-Jun, p21], or Kruskal–Wallis test followed by Dunn’s post hoc tests [ph-P53 (S15), p21, cleaved Casp3, Fodrin 120kDa]. $*p < 0.05$, $**p < 0.01$, $***p < 0.001$, $****p < 0.0001$ vs sham-injured animals; $\wedge p < 0.05$, $\wedge\wedge p < 0.01$, $\wedge\wedge\wedge p < 0.001$, $\wedge\wedge\wedge\wedge p < 0.0001$ vs CCI+Veh or inducer alone.

disrupt c-Jun (and caspase) activation, mithramycin is not neuroprotective in the C₂-ceramide model, suggesting these pathways are not among the dominant apoptosis-driving mechanisms in this model.

Using a mouse experimental TBI model (CCI), we detected acute DNA-damage responses⁶ and initiation of neuronal cell death mechanisms. Mithramycin modestly attenuated upregulation of some cell death pathways in the injured cortex 24 h after injury, including a significant reduction in levels of phosphorylated c-Jun (S63 and S73) and cleaved Fodrin fragments, and possible reduction in Puma and cleaved caspase-3. Brain Fodrin is primarily a neuronal protein⁴¹ whose cleavage is a neuronal death hallmark after acute brain injury^{75,76}. Depending on the neuronal environment, Fodrin may be cleaved to calpain/caspase-generated 145/150 kDa fragments or to a caspase-generated 120 kDa fragment whose predominance reflects strong caspase activity⁷⁷. Our previous studies showed repression of intrinsic caspase activation in the adult brain and low caspase activity acutely after experimental TBI^{62,78}. Appropriately, here we detected only modest effective caspase activation, indicated by prevalence of the more calpain-specific 145/150 kDa Fodrin fragments, and a far lower Caspase Activity Index at 24 h post-injury, compared with in vitro models.

Hence, CCI in adult mice may trigger neuronal cell death phenotypes other than intrinsic apoptosis such as those involving calpains⁷⁸. Our data show that mithramycin has more limited effects in calpain-dependent neuronal cell death including that induced by ceramide⁷⁹. Thus, while mithramycin may still attenuate some p53-dependent intrinsic apoptotic program elements, including BH3-only molecules, downstream cell death proteases and caspase-independent mechanisms as well as c-Jun activation, the narrower nature of these effects and relatively modest role played by the caspase-dependent portion of this cascade will likely reduce the neuroprotective therapeutic effect of mithramycin in *acute* TBI. However, as mithramycin acts upstream of MOMP, it may reduce

deleterious mitochondrial perturbations after TBI⁸⁰, leading to long-term protection. Also, progressive de-repression of intrinsic caspase activation pathways may occur after the acute phase⁶², increasing mithramycin’s therapeutic window.

In summary, we have demonstrated profound neuroprotection by mithramycin in DNA-damage-induced and p53-dependent neuronal cell death following in vitro exposure to widely used chemotherapy agents. We have also shown that these protective effects are partially recapitulated acutely in an in vivo model of brain trauma, consistent with the more limited role played by p53-dependent intrinsic apoptosis. Thus, mithramycin and other interventions targeting Sp1 may provide avenues for novel neuroprotective strategies particularly in conditions where pathological changes are driven by activation of c-Jun or the p53-dependent intrinsic apoptosis pathway.

Acknowledgements

This work was supported by National Institutes of Health (NIH) grants R01 NS091191 to A.I.F. and R01 NS096002 to B.A.S. and B.S. We are grateful for the technical support provided by Nicholas Braganca and Xiaoyi Lin.

Conflict of interest

The authors declare that they have no conflict of interest.

Publisher’s note

Springer Nature remains neutral with regard to jurisdictional claims in published maps and institutional affiliations.

Received: 31 March 2020 Revised: 6 July 2020 Accepted: 10 July 2020
Published online: 27 July 2020

References

- Dewan, M. C. et al. Estimating the global incidence of traumatic brain injury. *J. Neurosurg.* 1–18 <https://doi.org/10.3171/2017.10.JNS17352> (2018).
- Corrigan, J. D. et al. US population estimates of health and social outcomes 5 years after rehabilitation for traumatic brain injury. *J. Head. Trauma Rehabil.* **29**, E1–E9 (2014).
- Cruz-Haces, M., Tang, J., Acosta, G., Fernandez, J. & Shi, R. Pathological correlations between traumatic brain injury and chronic neurodegenerative diseases. *Transl. Neurodegener.* **6**, 20 (2017).

4. Gao, X. & Chen, J. Mild traumatic brain injury results in extensive neuronal degeneration in the cerebral cortex. *J. Neuropathol. Exp. Neurol.* **70**, 183–191 (2011).
5. Bramlett, H. M. & Dietrich, W. D. Long-term consequences of traumatic brain injury: current status of potential mechanisms of injury and neurological outcomes. *J. Neurotrauma* **32**, 1834–1848 (2015).
6. Smith, J. A., Park, S., Krause, J. S. & Banik, N. L. Oxidative stress, DNA damage, and the telomeric complex as therapeutic targets in acute neurodegeneration. *Neurochem Int* **62**, 764–775 (2013).
7. Ongnok, B., Chattipakorn, N. & Chattipakorn, S. C. Doxorubicin and cisplatin induced cognitive impairment: the possible mechanisms and interventions. *Exp. Neurol.* **324**, 113118 (2020).
8. El-Agamy, S. E., Abdel-Aziz, A. K., Esmat, A. & Azab, S. S. Chemotherapy and cognition: comprehensive review on doxorubicin-induced chemobrain. *Cancer Chemother. Pharm.* **84**, 1–14 (2019).
9. Elmore, S. Apoptosis: a review of programmed cell death. *Toxicol. Pathol.* **35**, 495–516 (2007).
10. Culmsee, C. & Mattson, M. P. p53 in neuronal apoptosis. *Biochemical Biophysical Res. Commun.* **331**, 761–777 (2005).
11. Aubrey, B. J., Kelly, G. L., Janic, A., Herold, M. J. & Strasser, A. How does p53 induce apoptosis and how does this relate to p53-mediated tumour suppression? *Cell Death Differ.* **25**, 104–113 (2018).
12. Hemann, M. & Lowe, S. The p53–Bcl-2 connection. *Cell Death Differ.* **13**, 1256–1259 (2006).
13. Graupner, V. et al. Differential regulation of the proapoptotic multidomain protein Bak by p53 and p73 at the promoter level. *Cell Death Differ.* **18**, 1130–1139 (2011).
14. García-Sáez, A. J. The secrets of the Bcl-2 family. *Cell Death Differ.* **19**, 1733–1740 (2012).
15. Shamas-Din, A., Kale, J., Leber, B. & Andrews, D. W. Mechanisms of action of Bcl-2 family proteins. *Cold Spring Harb. Perspect. Biol.* **5**, a008714 (2013).
16. Yu, J. & Zhang, L. The transcriptional targets of p53 in apoptosis control. *Biochemical Biophysical Res. Commun.* **331**, 851–858 (2005).
17. Suhaili, S. H., Karimian, H., Stellato, M., Lee, T.-H. & Aguilar, M.-I. Mitochondrial outer membrane permeabilization: a focus on the role of mitochondrial membrane structural organization. *Biophys. Rev.* **9**, 443–457 (2017).
18. Rink, A. et al. Evidence of apoptotic cell death after experimental traumatic brain injury in the rat. *Am. J. Pathol.* **147**, 1575–1583 (1995).
19. Clark, R. S. B. Detection of single- and double-strand DNA breaks after traumatic brain injury in rats: comparison of in situ labeling techniques using DNA polymerase I, the Klenow fragment of DNA polymerase I, and terminal deoxynucleotidyl transferase. *J. Neurotrauma* **18**, 675–689 (2001).
20. Plesnila, N. et al. Delayed neuronal death after brain trauma involves p53-dependent inhibition of NF- κ B transcriptional activity. *Cell Death Differ.* **14**, 1529–1541 (2007).
21. Huang, Y.-N. et al. Neuroprotective effects of pifithrin- α against traumatic brain injury in the striatum through suppression of neuroinflammation, oxidative stress, autophagy, and apoptosis. *Sci. Rep.* **8**, 2368 (2018).
22. Rachmany, L. et al. Cognitive impairments accompanying rodent mild traumatic brain injury involve p53-dependent neuronal cell death and are ameliorated by the tetrahydrobenzothiazole PFT- α . *PLoS ONE* **8**, e79837 (2013).
23. Di Giovanni, S. et al. The tumor suppressor protein p53 is required for neurite outgrowth and axon regeneration. *EMBO J.* **25**, 4084–4096 (2006).
24. Pennypacker, K. R. et al. NF- κ B p50 is increased in neurons surviving hippocampal injury. *Exp. Neurol.* **172**, 307–319 (2001).
25. Merlo, P. et al. p53 prevents neurodegeneration by regulating synaptic genes. *PNAS* **111**, 18055–18060 (2014).
26. Nikulenkov, F. et al. Insights into p53 transcriptional function via genome-wide chromatin occupancy and gene expression analysis. *Cell Death Differ.* **19**, 1992–2002 (2012).
27. Li, H. et al. Integrated high-throughput analysis identifies Sp1 as a crucial determinant of p53-mediated apoptosis. *Cell Death Differ.* **21**, 1493–1502 (2014).
28. Koutsodontis, G., Vasilaki, E., Chou, W.-C., Papakosta, P. & Kardassis, D. Physical and functional interactions between members of the tumour suppressor p53 and the Sp families of transcription factors: importance for the regulation of genes involved in cell-cycle arrest and apoptosis. *Biochem J.* **389**, 443–455 (2005).
29. Osada, N., Kosuge, Y., Ishige, K. & Ito, Y. Mithramycin, an agent for developing new therapeutic drugs for neurodegenerative diseases. *J. Pharmacol. Sci.* **122**, 251–256 (2013).
30. Ferrante, R. J. et al. Chemotherapy for the brain: the antitumor antibiotic mithramycin prolongs survival in a mouse model of huntington's disease. *J. Neurosci.* **24**, 10335–10342 (2004).
31. Lee, J. Y. et al. Improves functional recovery by inhibiting BSCB disruption and hemorrhage after spinal cord injury. *J. Neurotrauma* <https://doi.org/10.1089/neu.2017.5235> (2017).
32. Chatterjee, S., Zaman, K., Ryu, H., Conforto, A. & Ratan, R. R. Sequence-selective DNA binding drugs mithramycin A and chromomycin A3 are potent inhibitors of neuronal apoptosis induced by oxidative stress and DNA damage in cortical neurons. *Ann. Neurol.* **49**, 345–354 (2001).
33. Sleiman, S. F. et al. Mithramycin is a gene-selective Sp1 inhibitor that identifies a biological intersection between cancer and neurodegeneration. *J. Neurosci.* **31**, 6858–6870 (2011).
34. Riss, T. et al. in *Assay Guidance Manual* (Eli Lilly & Company and the National Center for Advancing Translational Sciences, 2019).
35. Sabirzhanov, B. et al. Downregulation of miR-23a and miR-27a following experimental traumatic brain injury induces neuronal cell death through activation of proapoptotic Bcl-2 proteins. *J. Neurosci.* **34**, 10055–10071 (2014).
36. Sabirzhanov, B. et al. miR-711 induced down-regulation of Angiopoietin-1 mediates neuronal cell death. *J. Neurotrauma* <https://doi.org/10.1089/neu.2017.5572> (2018).
37. Aubrecht, T. G. et al. Comparing effects of CDK inhibition and E2F1/2 ablation on neuronal cell death pathways in vitro and after traumatic brain injury. *Cell Death Dis.* **9**, 1121 (2018).
38. Clerc, P. & Polster, B. M. Investigation of mitochondrial dysfunction by sequential microplate-based respiration measurements from intact and permeabilized neurons. *PLoS ONE* **7**, e34465 (2012).
39. Livak, K. J. & Schmittgen, T. D. Analysis of relative gene expression data using real-time quantitative PCR and the 2⁻ $\Delta\Delta$ CT method. *Methods* **25**, 402–408 (2001).
40. Pfaffl, M. W. A new mathematical model for relative quantification in real-time RT-PCR. *Nucleic Acids Res.* **29**, e45 (2001).
41. Siman, R., Ahdoon, M. & Lynch, G. Ontogeny, compartmentation, and turnover of spectrin isoforms in rat central neurons. *J. Neurosci.* **7**, 55–64 (1987).
42. Fox, G. B., Fan, L., Levasseur, R. A. & Faden, A. I. Sustained sensory/motor and cognitive deficits with neuronal apoptosis following controlled cortical impact brain injury in the mouse. *J. Neurotrauma* **15**, 599–614 (1998).
43. Kabadi, S. V. et al. Selective CDK inhibitor limits neuroinflammation and progressive neurodegeneration after brain trauma. *J. Cereb. Blood Flow. Metab.* **32**, 137–149 (2012).
44. Kabadi, S. V. et al. CR8, a selective and potent CDK inhibitor, provides neuroprotection in experimental traumatic brain injury. *Neurotherapeutics* **9**, 405–421 (2012).
45. Loane, D. J. et al. Amyloid precursor protein secretases as therapeutic targets for traumatic brain injury. *Nat. Med.* **15**, 377–379 (2009).
46. Sokolowski, J. D. et al. Caspase-mediated cleavage of actin and tubulin is a common feature and sensitive marker of axonal degeneration in neural development and injury. *Acta Neuropathol. Commun.* **2**, 16 (2014).
47. Tapias, A., Ciudad, C. J., Roninson, I. B. & Noé, V. Regulation of Sp1 by cell cycle related proteins. *Cell Cycle* **7**, 2856–2867 (2008).
48. Piedrafitra, F. J. & Pfahl, M. Retinoid-induced apoptosis and Sp1 cleavage occur independently of transcription and require caspase activation. *Mol. Cell Biol.* **17**, 6348–6358 (1997).
49. Sabirzhanov, B. et al. miR-711 upregulation induces neuronal cell death after traumatic brain injury. *Cell Death Differ.* **23**, 654–668 (2016).
50. Muslimović, A., Nyström, S., Gao, Y. & Hammarsten, O. Numerical analysis of etoposide induced DNA breaks. *PLoS ONE* **4**, e85859 (2009).
51. Morris, E. J. & Geller, H. M. Induction of neuronal apoptosis by camptothecin, an inhibitor of DNA topoisomerase- α : evidence for cell cycle-independent toxicity. *J. Cell Biol.* **134**, 757–770 (1996).
52. Thorn, C. F. et al. Doxorubicin pathways: pharmacodynamics and adverse effects. *Pharmacogenet. Genom.* **21**, 440–446 (2011).
53. Deshmukh, M. & Johnson, E. M. Staurosporine-induced neuronal death: multiple mechanisms and methodological implications. *Cell Death Differ.* **7**, 250 (2000).
54. Czubowicz, K. & Strosznajder, R. Ceramide in the molecular mechanisms of neuronal cell death. The role of sphingosine-1-phosphate. *Mol. Neurobiol.* **50**, 26–37 (2014).
55. Zhu, W., Wang, X., Zhou, Y. & Wang, H. C2-ceramide induces cell death and protective autophagy in head and neck squamous cell carcinoma cells. *Int. J. Mol. Sci.* **15**, 3336–3355 (2014).

56. Ryu, H. et al. Sp1 and Sp3 are oxidative stress-inducible, antideath transcription factors in cortical neurons. *J. Neurosci.* **23**, 3597–3606 (2003).
57. Shroff, R. et al. Distribution and dynamics of chromatin modification induced by a defined DNA double-strand break. *Curr. Biol.* **14**, 1703–1711 (2004).
58. Siliciano, J. D. et al. DNA damage induces phosphorylation of the amino terminus of p53. *Genes Dev.* **11**, 3471–3481 (1997).
59. Nowshien, S. & Yang, E. S. The intersection between dna damage response and cell death pathways. *Exp. Oncol.* **34**, 243–254 (2012).
60. Siman, R. et al. Proteins released from degenerating neurons are surrogate markers for acute brain damage. *Neurobiol. Dis.* **16**, 311–320 (2004).
61. Clark, R. S. et al. Increases in Bcl-2 and cleavage of caspase-1 and caspase-3 in human brain after head injury. *FASEB J.* **13**, 813–821 (1999).
62. Yakovlev, A. G. et al. Differential expression of apoptotic protease-activating factor-1 and caspase-3 genes and susceptibility to apoptosis during brain development and after traumatic brain injury. *J. Neurosci.* **21**, 7439–7446 (2001).
63. Arai, M., Imamura, O., Kondoh, N., Dateki, M. & Takishima, K. Neuronal Ca²⁺-dependent activator protein 1 (NCDAP1) induces neuronal cell death by activating p53 pathway following traumatic brain injury. *J. Neurochem.* <https://doi.org/10.1111/jnc.14803> (2019).
64. Galluzzi, L. et al. Molecular mechanisms of cell death: recommendations of the Nomenclature Committee on Cell Death 2018. *Cell Death Differ.* **25**, 486–541 (2018).
65. Oda, E. et al. Noxa, a BH3-only member of the Bcl-2 family and candidate mediator of p53-induced apoptosis. *Science* **288**, 1053–1058 (2000).
66. Nakano, K. & Vousden, K. H. PUMA, a novel proapoptotic gene, is induced by p53. *Mol. Cell* **7**, 683–694 (2001).
67. Jung, Y.-S., Qian, Y. & Chen, X. Examination of the expanding pathways for the regulation of p21 expression and activity. *Cell. Signal.* **22**, 1003–1012 (2010).
68. Koutsodontis, G. & Kardassis, D. Inhibition of p53-mediated transcriptional responses by mithramycin A. *Oncogene* **23**, 9190–9200 (2004).
69. Thornborrow, E. C. & Manfredi, J. J. The tumor suppressor protein p53 requires a cofactor to activate transcriptionally the human BAX promoter. *J. Biol. Chem.* **276**, 15598–15608 (2001).
70. Karin, M., Liu, Z. & Zandi, E. AP-1 function and regulation. *Curr. Opin. Cell Biol.* **9**, 240–246 (1997).
71. Rumana, Akhter, Priyankar, Sanphui, Hrishita, Das, Pampa, Saha & Chandra, BiswasSubhas The regulation of p53 up-regulated modulator of apoptosis by JNK/c-Jun pathway in β -amyloid-induced neuron death. *J. Neurochemistry* **134**, 1091–1103 (2015).
72. Chen, B.-K. & Chang, W.-C. Functional interaction between c-Jun and promoter factor Sp1 in epidermal growth factor-induced gene expression of human 12(S)-lipoxygenase. *PNAS* **97**, 10406–10411 (2000).
73. Kim, B.-J. et al. In vitro and in vivo neuroprotective effects of cJun N-terminal kinase inhibitors on retinal ganglion cells. *Mol. Neurodegeneration* **11**, 30 (2016).
74. Kiryu-Seo, S. et al. Neuronal injury-inducible gene is synergistically regulated by ATF3, c-Jun, and STAT3 through the interaction with Sp1 in damaged neurons. *J. Biol. Chem.* **283**, 6988–6996 (2008).
75. Yokota, M., Saïdo, T. C., Tani, E., Kawashima, S. & Suzuki, K. Three distinct phases of fodrin proteolysis induced in postischemic hippocampus. Involvement of calpain and unidentified protease. *Stroke* **26**, 1901–1907 (1995).
76. Saïdo, T. C. et al. Spatial resolution of fodrin proteolysis in postischemic brain. *J. Biol. Chem.* **268**, 25239–25243 (1993).
77. Moore, J. D., Rothwell, N. J. & Gibson, R. M. Involvement of caspases and calpains in cerebrotical neuronal cell death is stimulus-dependent. *Br. J. Pharmacol.* **135**, 1069–1077 (2002).
78. Knoblach, S. M. et al. Caspase Inhibitor z-DEVD-fmk attenuates calpain and necrotic cell death in vitro and after traumatic brain injury. *J. Cereb. Blood Flow. Metab.* **24**, 1119–1132 (2004).
79. Prado Spalm, F. H. et al. Ceramide induces the death of retina photoreceptors through activation of parthanatos. *Mol. Neurobiol.* **56**, 4760–4777 (2019).
80. Cheng, G., Kong, R., Zhang, L. & Zhang, J. Mitochondria in traumatic brain injury and mitochondrial-targeted multipotential therapeutic strategies. *Br. J. Pharm.* **167**, 699–719 (2012).